Title

p62, Upregulated during Preneoplasia, Induces Hepatocellular Carcinogenesis by Maintaining Survival of Stressed HCC-Initiating Cells

Journal

Cancer Cell, 29(6)

ISSN

1535-6108

Authors

Umemura, Atsushi
He, Feng
Taniguchi, Koji
et al.

Publication Date

2016-06-01

DOI

10.1016/j.ccell.2016.04.006

Peer reviewed

Article

Cancer Cell

p62, Upregulated during Preneoplasia, Induces Hepatocellular Carcinogenesis by Maintaining Survival of Stressed HCC-Initiating Cells

Graphical Abstract

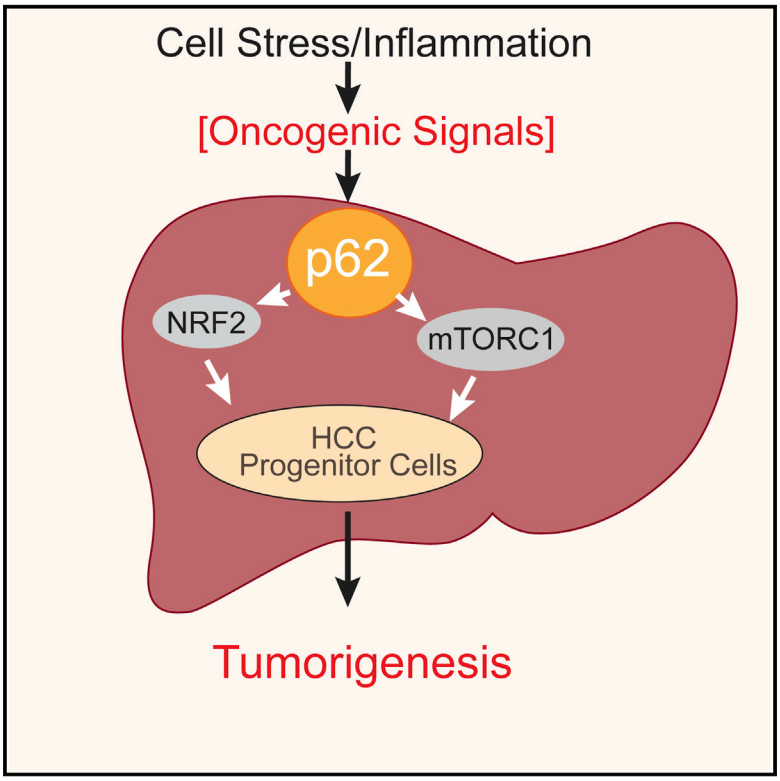

Authors

Atsushi Umemura, Feng He, Koji Taniguchi, ..., Maria T. Diaz-Meco, Jorge Moscat, Michael Karin

Correspondence

jmoscat@sbpdiscovery.org (J.M.), karinoffice@ucsd.edu (M.K.)

In Brief

Umemura et al. employ several mouse models of HCC to demonstrate that p62 facilitates activation of NRF2 and mTORC1 and is essential for HCC initiation. High levels of p62 accumulation in non-tumor liver tissue in early-stage HCC patients undergoing curative ablation correlates with reduced overall survival.

Highlights

- p62 in preneoplastic lesions is important for HCC development regardless of etiology
- Ectopic p62 expression is sufficient for HCC induction in autophagy-competent liver
- p62 exerts its oncogenic activity via NRF2 and mTORC1 but not via ubiquitin binding
- p62 promotes survival and expansion of ROS-containing HCC-initiating cells

Accession Numbers

GSE77323

Umemura et al., 2016, Cancer Cell *29*, 1–14
June 13, 2016
http://dx.doi.org/10.1016/j.ccell.2016.04.006

CellPress

Please cite this article in press as: Umemura et al., p62, Upregulated during Preneoplasia, Induces Hepatocellular Carcinogenesis by Maintaining Survival of Stressed HCC-Initiating Cells, Cancer Cell (2016), http://dx.doi.org/10.1016/j.ccell.2016.04.006

Cancer Cell
Article

p62, Upregulated during Preneoplasia, Induces Hepatocellular Carcinogenesis by Maintaining Survival of Stressed HCC-Initiating Cells

Atsushi Umemura,[1,5] Feng He,[1] Koji Taniguchi,[1,10,11] Hayato Nakagawa,[1,7] Shinichiro Yamachika,[1] Joan Font-Burgada,[1] Zhenyu Zhong,[1] Shankar Subramaniam,[3] Sindhu Raghunandan,[3] Angeles Duran,[9] Juan F. Linares,[9] Miguel Reina-Campos,[9] Shiori Umemura,[1,6] Mark A. Valasek,[2] Ekihiro Seki,[4,8] Kanji Yamaguchi,[5] Kazuhiko Koike,[7] Yoshito Itoh,[5] Maria T. Diaz-Meco,[9] Jorge Moscat,[9,*] and Michael Karin[1,2,*]

[1]Laboratory of Gene Regulation and Signal Transduction, Department of Pharmacology
[2]Department of Pathology
[3]Departments of Bioengineering, Cellular and Molecular Medicine, and Chemistry and Biochemistry
[4]Department of Medicine
University of California San Diego, 9500 Gilman Drive, La Jolla, CA 92093, USA
[5]Department of Molecular Gastroenterology and Hepatology
[6]Department of Obstetrics and Gynecology
Graduate School of Medical Science, Kyoto Prefectural University of Medicine, 465 Kajii-cho, Kawaramachi-Hirokoji, Kamigyo-ku, Kyoto 602-8566, Japan
[7]Department of Gastroenterology, Graduate School of Medicine, University of Tokyo, 7-3-1 Hongo, Bunkyo-ku, Tokyo 113-8655, Japan
[8]Division of Gastroenterology, Department of Medicine, Cedars-Sinai Medical Center, 8700 Beverly Boulevard, Los Angeles, CA 90048, USA
[9]Cancer Metabolism and Signaling Networks Program, Sanford-Burnham-Prebys Medical Discovery Institute, 10901 North Torrey Pines Road, La Jolla, CA 92037, USA
[10]Department of Surgery and Science, Graduate School of Medical Sciences, Kyushu University, Fukuoka 812-8582, Japan
[11]Department of Microbiology and Immunology, Keio University School of Medicine, Tokyo 160-8582, Japan
*Correspondence: jmoscat@sbpdiscovery.org (J.M.), karinoffice@ucsd.edu (M.K.)
http://dx.doi.org/10.1016/j.ccell.2016.04.006

SUMMARY

p62 is a ubiquitin-binding autophagy receptor and signaling protein that accumulates in premalignant liver diseases and most hepatocellular carcinomas (HCCs). Although p62 was proposed to participate in the formation of benign adenomas in autophagy-deficient livers, its role in HCC initiation was not explored. Here we show that p62 is necessary and sufficient for HCC induction in mice and that its high expression in non-tumor human liver predicts rapid HCC recurrence after curative ablation. High p62 expression is needed for activation of NRF2 and mTORC1, induction of c-Myc, and protection of HCC-initiating cells from oxidative stress-induced death.

INTRODUCTION

Despite extensive exploration, cancer initiation remains obscure. Most neoplasms form in response to environmental carcinogens that induce cancer-initiating mutations (Luch, 2005). In some cases, e.g., colorectal cancer, these mutations occur in rapidly dividing adult tissue stem cells (van de Weteringet al., 2015), but in other cases, such as hepatocellular carcinoma (HCC), cancer likely emerges from terminally differentiated cells (Font-Burgada et al., 2015). Since a typical cancer requires two to eight driver mutations (Vogelstein et al., 2013), cancer-initiating cells should survive environmental insults, divide, and give rise to a cluster of initiated cells that remain insult resistant and thus capable of accumulating

Significance

p62 is the main component of Mallory-Denk bodies and hyaline granules that are present in the majority of premalignant liver diseases and HCC. Our results indicate that p62 accumulation is required for progression from premalignancy to malignancy, most likely by preventing oxidative stress-induced death of HCC-initiating cells, thereby allowing such cells to accumulate multiple oncogenic mutations. Hepatocyte-specific p62 expression promotes c-Myc induction and NRF2 and mTORC1 activation. Therefore, p62 levels serve as a strong prognostic indicator of rapid HCC recurrence after curative ablation.

additional mutations. However, how cancer-initiating cells escape death to keep accumulating driver mutations has not been fully investigated.

A common malignancy linked to chronic tissue damage, stress, and environmental carcinogen exposure is HCC, most of which arises as the end stage of chronic liver disease and persistent inflammation, with hepatitis B or C virus (HBV, HCV) infections being the current leading causes (El-Serag, 2011). However, obesity and alcohol consumption, which cause hepatic steatosis (non-alcoholic steatohepatitis [NASH] or alcoholic steatohepatitis [ASH], respectively) and fibrosis, are rapidly growing in their importance as HCC risk factors (Starley et al., 2010). Mouse studies show that obesity promotes HCC through inflammation-related mechanisms (Nakagawa et al., 2014; Park et al., 2010; Wolf et al., 2014), but it is unclear how diverse forms of hepatitis and liver damage initiate HCC. Identification of a common pathogenic pathway is important for early HCC detection and improved prevention.

The heterogeneous nature of HCC, in which over 28,000 different somatic mutations have been identified (Schulze et al., 2015; Shibata and Aburatani, 2014), renders early detection and prevention challenging. Most HCCs exhibit a median of 21 silent and 64 non-silent mutations that affect 8–11 major signaling pathways and biological processes, including cellular stress responses (Schulze et al., 2015; Shibata and Aburatani, 2014). Stress responses are elicited by ER and oxidative stresses, viral hepatitis, hemochromatosis, and ASH and NASH (Malhi and Kaufman, 2011; Starley et al., 2010), and they control NASH to HCC progression in mice (Nakagawa et al., 2014). ER stress enhances oxidative stress, which is relieved by nuclear factor erythroid 2 (NRF2) by inducing expression of genes encoding antioxidant and detoxifying enzymes (Suzuki et al., 2013). NRF2 is regulated post-translationally by the E3 ubiquitin ligase Keap1, which induces NRF2 ubiquitination and proteasomal degradation. Upon accumulation of reactive oxygen species (ROS) or electrophiles, Keap1 is oxidized and unable to bind newly translated NRF2, which is stabilized and enters the nucleus to activate genes harboring antioxidant response elements. Because products of NRF2-regulated genes detoxify electrophiles and promote glutathione synthesis, transient activation of this system was proposed to inhibit carcinogenesis in liver and other organs (Hayes and McMahon, 2009; Suzuki et al., 2013). Surprisingly, however, *KEAP1* inactivating mutations occur in lung cancer and HCC (Ohta et al., 2008; Schulze et al., 2015; Totoki et al., 2014), and activating mutations in the gene encoding NRF2, *NFE2L2*, that inhibit Keap1-mediated degradation were found in lung, esophageal, skin, and liver cancers (Guichard et al., 2012; Kim et al., 2010; Shibata et al., 2008). Together, *NFE2L2* and *KEAP1* mutations occur in 14% of HCC specimens and are considered to be driver mutations (Schulze et al., 2015; Shibata and Aburatani, 2014; Totoki et al., 2014). NRF2 was proposed to contribute to liver carcinogenesis by inhibiting senescence or death of initiated hepatocytes undergoing oxidative stress (Hayes and McMahon, 2006), but direct support for this hypothesis, first postulated by Farber (1990), is lacking. Curiously, carcinogen-induced dysplastic lesions in rats, known as foci of altered hepatocytes (FAH), express high amounts of glutathione S-transferase P1 (Gstp1), NAD(P)H:quinone oxidoreductase 1 (Nqo1), and other protective enzymes (Farber, 1990), now known as NRF2 targets (Hayes and McMahon, 2009). As a result, FAH are probably more resistant to oxidative stress and environmental toxins than the surrounding liver. Thus, antioxidants may promote rather than suppress HCC development, as previously found (Maeda et al., 2005). It was also questioned whether FAH, also found in human cirrhotic and preneoplastic livers, are true HCC progenitors or reflect compensatory proliferation triggered by liver damage (Sell and Leffert, 2008). We have settled this controversy by isolating small hepatocytic cells from mouse dysplastic lesions that give rise to HCC after transplantation into a damaged liver (He et al., 2013). In addition to cancer stem cell markers, HCC progenitor cells (HcPC) exhibit elevated p62, which also accumulates in livers of high-fat diet (HFD)-fed MUP-uPA mice that develop NASH and progress to HCC (Nakagawa et al., 2014). p62 is known to accumulate in most, if not all, chronic liver diseases that progress to HCC (Denk et al., 2006).

p62, encoded by *SQSTM1*, is an autophagy adaptor and a signaling scaffold with an N-terminal oligomerization domain (PB1) and a ubiquitin association domain (UBA) at its C terminus (Komatsu et al., 2012). p62 also harbors light-chain protein 3 (LC3) motif and Keap1 interacting motif (KIR), through which it binds LC3 on phagophore membranes and cytoplasmic Keap1, respectively. A main p62 function is to deliver polyubiquitinated proteins and organelles for autophagosomal-lysosomal degradation. Interference with autophagic flux attenuates p62 degradation (Komatsu et al., 2012). The latter results in p62 accumulation and oligomerization, aggregation of ubiquitinated proteins, Keap1 titration, and NRF2 stabilization. As NRF2 can induce p62 expression (Jain et al., 2010), p62 accumulation can trigger a self-amplifying autoregulatory loop that sustains NRF2 activation and p62 overexpression. p62 also binds TRAF6 to promote nuclear factor κB (NF-κB) activation (Sanz et al., 2000), and NF-κB can also induce p62 expression (Ling et al., 2012). Under nutrient-rich conditions, the p62/TRAF6 interaction also enhances mammalian target of rapamycin complex 1 (mTORC1) activation (Duran et al., 2011; Linares et al., 2013). Importantly, p62 is a major component of intracellular hyaline bodies, Mallory-Denk bodies (MDB), and hybrid inclusions (Denk et al., 2006), which are hallmarks of chronic liver diseases that greatly enhance HCC risk (Zatloukal et al., 2007). p62-containing aggregates have been detected in 50% of surgical HCC specimens (Denk et al., 2006), but their significance remains unknown. Of note, whole-body p62 disruption suppresses benign adenomas in autophagy-deficient livers (Takamura et al., 2011). These tumors, however, are not cancerous and thus the role of p62 and its mechanism of action in HCC initiation remain unknown, although it was shown that p62 maintains malignancy of HCC cell lines (Ichimura et al., 2013; Inami et al., 2011). p62 has been suggested to act as an oncoprotein in renal cell carcinoma by promoting mTORC1 activation (Li et al., 2013), while other studies have suggested it acts via NF-κB or oxidative stress (Mathew et al., 2009). p62 also accumulates in endometrial cancer (Iwadate et al., 2015). Yet in no case was it investigated whether p62 accumulation in a preneoplastic tissue increases the risk of cancer initiation.

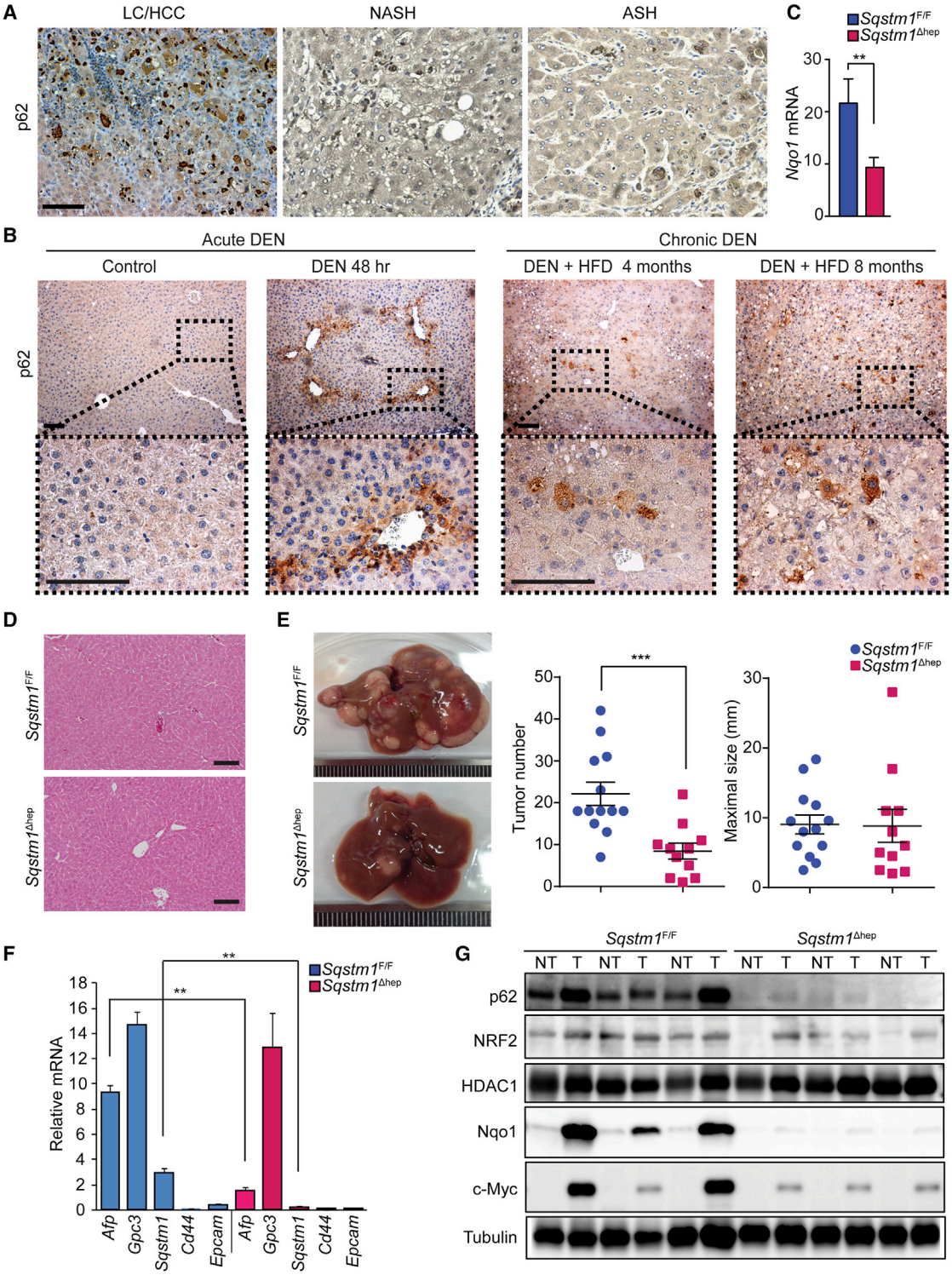

Figure 1. Diminished DEN-Induced Hepatocarcinogenesis in *Sqstm1*$^{\Delta hep}$ Mice

(A) p62-positive aggregates in human LC/HCC (liver cirrhosis/HCC), NASH, and ASH specimens (n = 3).

(B) Left: rapid p62 induction in mouse livers (n = 3) after high-dose DEN (100 mg/kg body weight [BW]). Right: chronic p62 expression in mouse livers (n = 3) after low-dose DEN (25 mg/kg BW) and HFD feeding.

(C) *Nqo1* liver mRNA expression 48 hr after DEN injection analyzed by qPCR. Results are mean ± SD (n = 3).

(D) H&E staining of *Sqstm1*$^{F/F}$ and *Sqstm1*$^{\Delta hep}$ livers (n = 4).

(legend continued on next page)

RESULTS

p62 Is Induced by Diethylnitrosamine and Enhances Its Carcinogenic Activity

We confirmed p62 accumulation in human patients suffering from chronic liver diseases that increase HCC risk, as well as HCC itself (Figure 1A). Consistent with this, in mice p62 was rapidly induced in liver after challenge with a high dose of diethylnitrosamine (DEN) (100 mg/kg), mainly around the central vein (Figure 1B), the area within which DEN undergoes metabolic activation (Kang et al., 2007). A carcinogenic DEN dose (25 mg/kg) followed by HFD feeding also led to p62 accumulation, but this time the process was slower and after 2–4 months only a few hepatocytic cell clusters were high in p62 (Figures 1B and S1A). At later time points p62-high cells were mainly restricted to tumor nodules, and no differences in p62 expression were noted between mice given DEN alone or DEN plus HFD. To determine p62's role in hepatocarcinogenesis, we generated *Sqstm1*$^{\Delta hep}$ mice lacking p62 in hepatocytes (Figure S1B). Immunoblot (IB) analysis revealed complete absence of p62 protein, and qPCR analysis showed reduced *Nqo1* mRNA induction after DEN challenge (Figures 1C and S1C). The *Sqstm1*$^{\Delta hep}$ liver, however, was phenotypically normal and did not display any damage (Figure 1D). Two-week-old *Sqstm1*$^{\Delta hep}$ males given DEN alone or DEN plus HFD (Park et al., 2010) developed 55% fewer HCCs than similarly treated *Sqstm1*$^{F/F}$ mice (Figures 1E and S1D). Maximal tumor size, however, remained unchanged; suggesting that p62 mainly affects tumor initiation rather than growth. p62-Deficient HCCs expressed less α-fetoprotein (AFP) than p62-proficient HCCs, but glypican 3 (GPC3) remained unchanged (Figures 1F and S1E), suggesting that p62-deficient tumors contain fewer poorly differentiated cells. All DEN-induced tumors were histologically typical HCCs, as previously found (Maeda et al., 2005). IB analysis confirmed that most HCCs in *Sqstm1*$^{F/F}$ mice displayed high p62 expression, which was also seen in non-tumor areas (Figure 1G). p62 expression generally correlated with NRF2 stabilization and elevated Nqo1 expression (Figures 1G and S1F). p62-Deficient tumors expressed much less Nqo1 protein (Figures 1G and S1E). p62 deletion reduced tumoral expression of NRF2 targets, including *Hmox1*, *Gstm1*, and *Nqo1* mRNAs (Figure S1F). c-Myc expression, which is frequently elevated in HCC (Kaposi-Novak et al., 2009; Qu et al., 2014), also correlated with elevated p62 (Figure 1G).

p62 Is Required for HCC Initiation in *Tsc1*$^{\Delta hep}$ Mice

Tsc1$^{\Delta hep}$ male mice, in which hepatocyte mTORC1 is constitutively activated, exhibit spontaneous HCC development preceded by fibrosis, liver damage, and p62 accumulation (Menon et al., 2012). mTORC1 activation, however, is dispensable for DEN-induced HCC; in fact *Rptor*$^{\Delta hep}$ mice exhibit enhanced HCC development (Umemura et al., 2014). To determine whether p62 participates in mTORC1-driven hepatocarcinogenesis, we generated *Tsc1*$^{\Delta hep}$ mice, which developed typical HCCs as described above, and crossed them with *Sqstm1*$^{\Delta hep}$ mice to generate *Tsc1*/*Sqstm1*$^{\Delta hep}$ double mutants (Figures 2A and S2A). p62 ablation did not restore LC3 lipidation but reduced p70S6 kinase (S6K) phosphorylation. Remarkably, liver-specific p62 ablation completely suppressed HCC development (Figure 2B). As expected, p62 was upregulated in non-tumor and tumor areas of *Tsc1*$^{\Delta hep}$ liver, and its upregulation correlated with enhanced NRF2, c-Myc, and NRF2 target gene expression (Figures 2C and 2D). p62 ablation in *Tsc1*$^{\Delta hep}$ liver reduced S6K and S6 phosphorylation, suggesting decreased mTORC1 activity (Figures 2A, 2C, and S2B). However, restoration of AKT phosphorylation, which is inhibited upon S6K activation (Hay and Sonenberg, 2004), was variable (Figures 2A and 2C). p62 ablation reduced expression of fibrogenic genes and the Yes-associated protein (YAP) targets connective tissue growth factor (*Ctgf*) and amphiregulin (*Areg*), which are upregulated in the *Tsc1*$^{\Delta hep}$ liver (Figure 2D). Inflammation and fibrotic changes were also reduced in the *Tsc1*/*Sqstm1*$^{\Delta hep}$ liver relative to *Tsc1*$^{\Delta hep}$ livers (Figure S2B). Of note, p62 ablation reduced the abundance of ROS-accumulating cells that are stained by dihydroethidine (DHE) (Figure S2B). Consistent with increased S6K activation, *Tsc1*$^{\Delta hep}$ HCCs exhibited elevated S6 phosphorylation and c-Myc (Figure S2C).

p62 Accelerates NASH to HCC Progression

Hypernutrition activates mTORC1 resulting in inhibitory ULK1/2 phosphorylation, reduced autophagic flux, and p62 accumulation (Schneider and Cuervo, 2014). We developed a new mouse model of NASH-driven HCC by feeding MUP-uPA mice with HFD, which induces p62 accumulation in non-tumor liver and HCCs (Nakagawa et al., 2014). Surprisingly, HFD feeding to wild-type (WT) B6 mice, which do not develop NASH or HCC, did not induce p62 accumulation (Figure 3A). In contrast, HFD induced strong p62 expression in MUP-uPA mice (Figure 3A), suggesting that p62 accumulation is tightly linked to NASH and HCC development. To probe the pathogenic role of p62, we crossed MUP-uPA and *Sqstm1*$^{\Delta hep}$ (*Sqstm1*$^{\Delta hep}$/MUP) mice and placed male progeny on HFD. Although p62 ablation did not decrease liver lipid droplets or triglycerides, it led to reduced fibrosis and nearly complete absence of cells that accumulate superoxides, which are DHE positive (Figures 3B–3D). Notably, p62 ablation substantially suppressed HCC development (Figure 3E). Both tumor number and maximal size were reduced in *Sqstm1*$^{\Delta hep}$/MUP mice, and no p62 expression was seen in the remaining tumors (Figure 3B).

NASH development and HCC progression is also seen in the STZ-HFD model, based on induction of type 1 diabetes (β-cell destruction) with streptozotocin (STZ) followed by HFD feeding (Kawai et al., 2012). STZ-HFD mice develop HCC, whose histological features were similar to those of HCC in MUP-uPA mice, including p62 accumulation. Although p62 deletion in the STZ-HFD model did not suppress fibrosis, steatosis, or triglyceride accumulation, it strongly suppressed HCC development (Figures S3A–S3D).

(E) Gross appearance, tumor multiplicity, and maximal sizes of DEN-induced HCCs. Results are mean ± SEM (n = 11–13).
(F) Relative mRNA amounts of HCC and progenitor markers as well as *Sqstm1* in tumors from DEN-injected mice. Results are mean ± SD (n = 4).
(G) IB analysis of p62, nuclear NRF2, HDAC1, Nqo1, c-Myc, and tubulin in tumor (T) and non-tumor (NT) liver tissue from DEN-injected mice (n = 5–6).
**p < 0.01, ***p < 0.001. Scale bars, 100 μm. See also Figure S1.

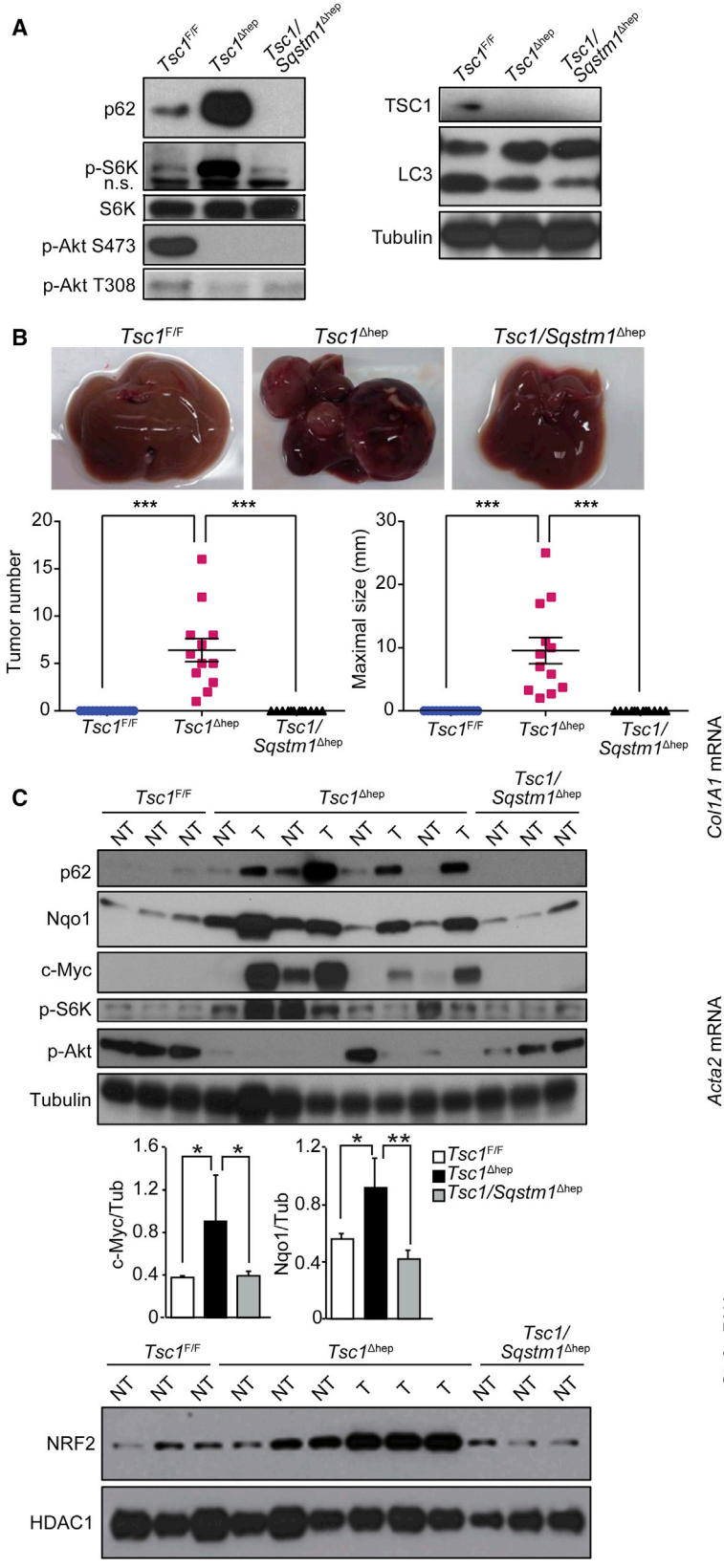

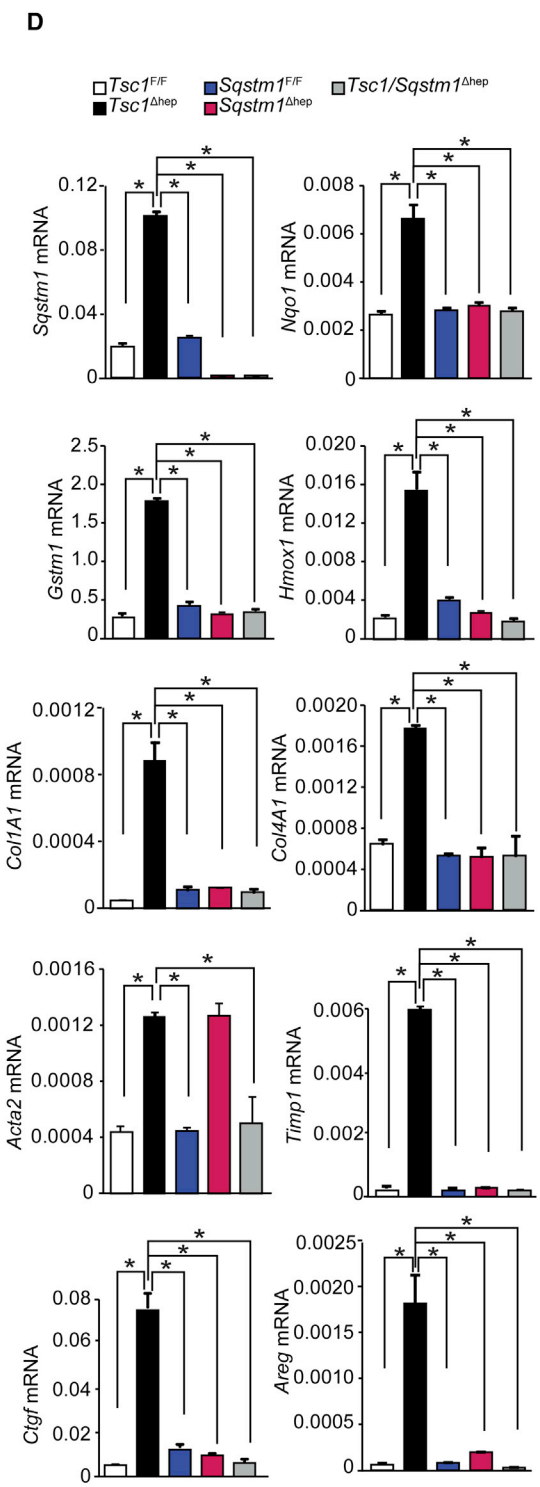

(legend on next page)

Ectopic p62 Expression Induces HCC

We examined whether ectopic p62 expression can induce HCC without carcinogen administration, hypernutrition, or deliberate tissue injury. We generated plasmid vectors expressing GFP and FLAG-tagged p62 proteins, either full-length (FL), KIR-deficient (KIR^-), or UBA-deleted (ΔUBA) (Figure 4A). Transfected mouse hepatocytes exhibited efficient expression of all three p62 variants (Figures 4B and 4C). Whereas p62 FL and p62 KIR^- formed aggregates, the ΔUBA construct did not (Figure 4C). p62 FL and p62 ΔUBA, but not p62 KIR^-, induced endogenous NRF2 targets, including *Nqo1* and *Hmox1* (Figures 4B and S4A). We transferred the different constructs into adeno-associated virus (AAV) serotype 8 vectors, which exhibit strong liver tropism and stably express ectopic proteins, and confirmed that GFP was efficiently expressed in hepatocytes for at least 12 months after AAV infection (Figure S4B). Ectopic p62 was expressed in cells expressing the FLAG epitope (Figure S4C). Notably, p62 FL and p62 ΔUBA induced tumors with either steatotic or typical HCC morphologies at 12 months after infection of WT male mice (Figures 4D and S4D). Tumor multiplicity was 50% of that seen in HFD-fed MUP-uPA mice. No significant differences between tumor multiplicity were observed between p62 FL and p62 ΔUBA infected mice, although tumors in the latter were somewhat smaller, and no tumors were observed in mice receiving p62 KIR^- (Figure 4D). Only one mouse infected with AAV-GFP and kept on HFD developed a tumor at 12 months. Although AAV injection into mice was reported to induce occasional liver tumors, these tumors were found at 14–25 months after infection (Chandler et al., 2015), well beyond the time point at which we examined our mice. Some p62-induced tumors exhibited lipid droplets, ballooning deformity, and MDB, which are common features of steatohepatic HCCs (Figure S4D). All p62-induced HCCs expressed exogenous and endogenous p62 and FLAG epitope, together with elevated NRF2 and Nqo1 (Figure 4E). S6K phosphorylation and c-Myc were elevated, but the LC3-II/LC3-I ratio remained high (Figure 4E). This was markedly different from $Atg7^{\Delta hep}$ liver in which p62 was strongly induced and autophagy was completely blocked, but phospho-S6K was not elevated. p62-Induced tumors were positive for HCC markers, including GPC3, AFP, and YAP (Figures 4F and S4E). These tumors also included a small number of Sox9-positive cells. Tumor nodules were positive for p62 and the FLAG epitope, as well as phospho-S6, but were negative for nuclear RelA (Figures 4F and S4E).

Liver p62 Controls NRF2 and mTORC1/c-Myc Signaling

We performed RNA sequencing (RNA-seq) on $Sqstm1^{\Delta hep}$ and $Sqstm1^{F/F}$ livers to identify differentially expressed genes and signaling pathways that are strongly influenced by p62. Ingenuity pathway analysis revealed that the NRF2-mediated oxidative stress response was the highest-ranking downregulated pathway in the $Sqstm1^{\Delta hep}$ liver (Figure 5A). Heatmap depiction shows downregulated "NRF2-mediated Oxidative Stress Response"-related genes, including *Cbr1*, *Gstm5*, *Abcc4*, *Nqo1*, and *Gpx2* in $Sqstm1^{\Delta hep}$ liver (Figure 5B). qPCR analysis of additional NRF2 genes revealed marked reduction of this pathway (Figure S5A). The products of these genes are involved in glutathione metabolism, antioxidant defenses, and electrophile detoxification. c-Fos, which was implicated as a key contributor to HCC pathogenesis (Min et al., 2012), was also downregulated in $Sqstm1^{\Delta hep}$ liver. We conducted similar analyses on $Tsc1^{\Delta hep}$ and $Tsc1/Sqstm1^{\Delta hep}$ livers. Again, p62 ablation reduced expression of NRF2-regulated genes (Figure 5C). In this case, however, gene set enrichment analysis (GSEA) of RNA-seq data indicated that p62 ablation also reduced expression of c-Myc- and mTORC1-responsive genes (Figures 5D and 5E), in agreement with its effects on S6K phosphorylation and c-Myc expression.

We also investigated *SQSTM1* mRNA expression in different HCC datasets (Oncomine and The Cancer Genome Atlas [TCGA]), six of which showed higher *SQSTM1* mRNA in HCC than in normal tissue (Figure S5B). We chose the largest and most completely annotated TCGA dataset and performed GSEA of correlation profiles. Analyses with the C3 compilation of the Molecular Signatures Database revealed that among genes directly correlated with *SQSTM1*, there is a striking enrichment for genes controlled by NRF2, including a strong positive correlation with *NQO1* (Figures S5C–S5E). Further analysis of the TCGA dataset revealed a significant tendency toward co-occurrence between *SQSTM1* overexpression and *NQO1* and *GPX2* (Figure S5F). GSEA of these data also revealed good correlation between *SQSTM1* and *MYC*- and mTORC1-responsive genes (Figures S5G and S5H). Furthermore, silencing of p62 in an established human HCC cell line confirmed the relationship between elevated *SQSTM1* and increased *MYC* and *NQO1* expression and S6K phosphorylation (Figures S5I and S5J).

p62 Accumulation Correlates with HCC Recurrence

We investigated the relationship between p62 accumulation and human HCC risk by analyzing non-tumor liver tissue of early-stage HCC patients undergoing curative ablation. The results were graded from 0 to 3 depending on average number of p62-positive aggregates per field (Figure 6A). Remarkably, 79 out of 121 specimens were p62 positive. We next analyzed disease-free survival (in years) in the same patients (Figure 6B). Disease-free survival was much worse in patients with high-grade p62 in non-tumor liver than in patients with low or no p62 staining. Moreover, the p62 staining index positively correlated with fibrosis score and liver stiffness assessed by

Figure 2. p62 Ablation Blocks HCC Development in $Tsc1^{\Delta hep}$ Mice

(A) IB analysis of liver tissues from indicated mice (n = 4–6). n.s., nonspecific band.

(B) Upper: gross liver morphology of 10-month-old male mice of indicated genotypes. Lower: tumor numbers and maximal sizes (n = 12–16). Results are mean ± SEM.

(C) IB analysis and quantitation of protein expression and phosphorylation in tumor (T) and non-tumor (NT) liver tissue. Results are mean ± SD (n = 3–4).

(D) qPCR analysis of relative mRNA levels of *Sqstm1*, NRF2 targets (*Nqo1*, *Gstm1*, *Hmox1*), fibrogenic markers (*Col1A1*, *Col4A1*, *Acta2*, *Timp1*) and YAP targets (*Ctgf* and *Areg*) in livers of 10-month-old mice (n = 3–4 per genotype). Results are mean ± SD.

*p < 0.05, **p < 0.01, ***p < 0.001. See also Figure S2.

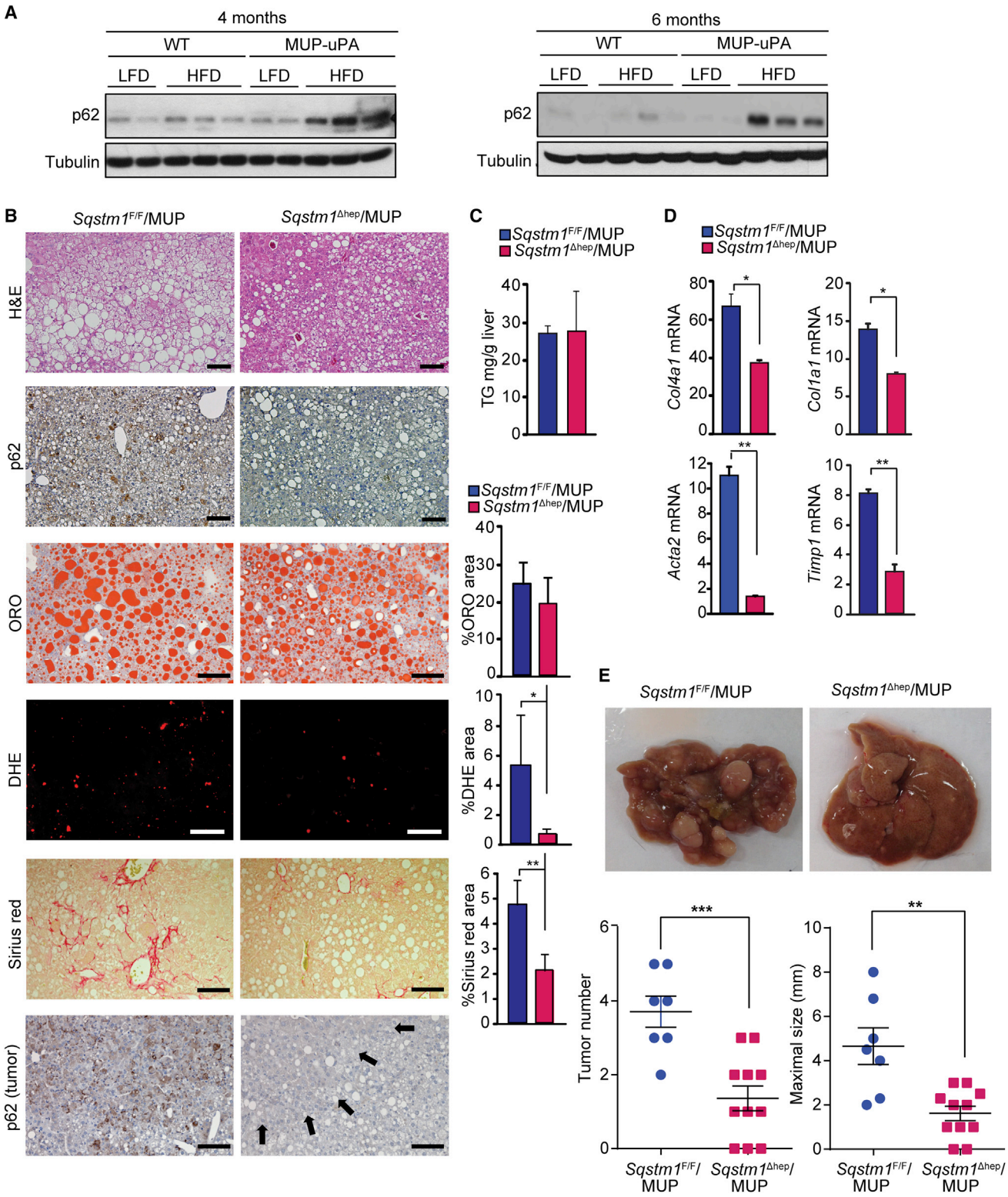

Figure 3. p62 Ablation Prevents HCC Development but Not Steatosis in MUP-uPA Mice

(A) IB analysis of liver tissue lysates from BL6 (WT) and MUP-uPA mice of indicated ages kept on a LFD or an HFD (n = 2–3).

(B) Histochemistry of livers from 5-month-old mice kept on HFD. Lower panel shows p62 staining in tumors of 10-month-old mice on HFD. Arrows indicate tumor portion. Graphs indicate percentage of areas occupied by stained cells. Results are mean ± SD (n = 3–5). Scale bars, 100 μm.

(legend continued on next page)

histology and transient elastography, respectively (Figure 6C). These results suggest that p62 is a useful biomarker for the risk of HCC recurrence that can be used to identify patients who should be closely monitored after curative HCC ablation. Kaplan-Meier survival analysis of patients stratified according to *SQSTM1* expression, whose data was included in the Oncomine and TCGA datasets, revealed that high *SQSTM1* expression correlated with significantly worse patient survival (Figures S6A and S6B).

DISCUSSION

Cancer often develops in tissues, such as liver, with very low rates of inherent cell division. Injury and inflammation promote such cancers by enhancing proliferation of initiated cells (Finkin et al., 2015; Grivennikov et al., 2010; Kuraishy et al., 2011), but mechanisms that increase cancer risk and operate prior to acquisition of oncogenic mutations are obscure. It is not even clear how the progeny of a single initiated cell can acquire the multiple mutations needed for malignant transformation. Studying HCC, a cancer that most likely originates from differentiated hepatocytes (Font-Burgada et al., 2015), we find that accumulation of p62, a marker of chronic liver disease (Denk et al., 2006), is an early event that sets up a "field effect" within which HCC evolves. "Field cancerization" is a poorly understood process that occurs prior to emergence of neoplasia, during which a histologically invisible change renders part of a tissue highly likely to develop malignant tumors (Rubin, 2011). We show that p62 accumulation precedes HCC development in mice and humans and suggest it is responsible for increasing cancer risk by supporting survival and accumulation of ROS-containing HcPC, the cells in which HCC-driver mutations occur.

Although p62 was upregulated in autophagy-deficient livers and p62 ablation attenuated the genesis of benign hepatic adenomas (Takamura et al., 2011), and inhibited proliferation and growth of established HCC cell lines (Ichimura et al., 2013; Inami et al., 2011), the role of p62 in HCC initiation within a precancerous liver was not investigated. We now show that in human patients with early HCC p62 accumulation in non-tumor liver correlates with much faster post-therapeutic recurrence and reduced disease-free survival. Hence, patients with high p62 expression in non-tumor tissue need closer surveillance and additional intervention. Using four distinct mouse HCC models of differing etiology, we show that p62 is needed for initiation of malignant tumors with classical HCC features. The most dramatic dependence on p62 was exhibited by $Tsc1^{\Delta hep}$ mice, in which HCC development depends on mTORC1 (Menon et al., 2012), which is also activated by hypernutrition, causing attenuation of autophagy and p62 accumulation (Schneider and Cuervo, 2014). Nonetheless, HFD feeding causes p62 accumulation in MUP-uPA and STZ but not in WT mice. Thus, p62 is not linked to development of steatotic changes; rather, it is strictly required for NASH to HCC progression. Our results also indicate that p62 accumulation can initiate HCC development, suggesting it is a critical preneoplastic event that leads to non-mutational activation of three important cancer drivers: NRF2, mTORC1, and c-Myc.

Pathogenic p62 accumulation in premalignant liver tissue is regulated transcriptionally and post-transcriptionally. The major activators of p62 transcription, NRF2 and NF-κB (Jain et al., 2010; Ling et al., 2012), are activated during chronic liver inflammation and oxidative stress (Figure 7). In turn, p62 can activate NF-κB (Sanz et al., 2000) and NRF2 (Ichimura et al., 2013), constituting two self-amplifying autoregulatory loops. In our experimental system, exogenous p62 activated NRF2, and this may have induced endogenous p62, thereby explaining preferential p62 accumulation within tumor nodules. Even when initial p62 expression is relatively uniform, small fluctuations can generate foci of high p62 concentrations. Given the ability of p62 to activate NRF2, these are probably the preneoplastic foci previously detected by virtue of Nqo1 or Gstp1 (a marker of rat, but not mouse, FAH) expression (Farber, 1990; Hayes and McMahon, 2006).

Elevated *SQSTM1* mRNA is insufficient for formation of p62-containing aggregates, because a major factor that dictates p62 protein amounts is autosomal-lysosomal proteolysis (Komatsu et al., 2012). Dramatic p62 upregulation is seen after ATG5 or ATG7 ablation, although the complete absence of either protein in the liver prevents malignant HCC development. Therefore, only partial inhibition of autophagy is compatible with progression of p62-expressing FAH to malignant HCC. Such conditions occur during NASH development or in $Tsc1^{\Delta hep}$ mice, whereby autophagy is partially inhibited due to mTORC1 activation. However, modest mTORC1 activation induced by HFD does not cause p62 accumulation and malignant progression. Other conditions that lead to p62 accumulation are inflammation and oxidative stress (Figure 7), which are general features of chronic liver disease along with reduced autophagic flux (Czaja, 2011; Schneider and Cuervo, 2014).

Previous work attributed pro-tumorigenic p62 activity to mTORC1 (Li et al., 2013; Linares et al., 2015). Elevated S6K phosphorylation, indicative of mTORC1 activation, is also seen in HCC nodules induced by ectopic p62, whereas p62 ablation in $Tsc1^{\Delta hep}$ mice reduces S6K phosphorylation. However, AKT T308 or S473 phosphorylation, which is suppressed upon S6K activation, is only weakly and inconsistently restored by p62 ablation, suggesting that other signaling pathways contribute to hepatic insulin resistance. One likely contributor is the JNK pathway, which is activated during HCC development (Nakagawa et al., 2014; Sakurai et al., 2006) and inhibits insulin-activated AKT (Solinas et al., 2006). These data support the notion that p62-dependent liver tumorigenesis may be mediated in part via mTORC1. Dependence on mTORC1, however, does not apply to the DEN model, where Raptor ablation enhances, rather than suppresses, HCC development (Umemura et al., 2014). Another oncogenic mediator induced by p62 is c-Myc, a known player in HCC development (Shibata and Aburatani, 2014). As seen with p70S6, c-Myc expression and activity in mouse and human HCC

(C) Liver triglyceride (TG) content of 5-month-old mice on HFD. Results are mean ± SD (n = 4).
(D) Relative mRNA amounts of fibrogenic markers in mice of indicated genotypes. Results are mean ± SD (n = 4).
(E) Gross liver morphology (upper) and tumor numbers and maximal sizes (lower) in 10-month-old mice kept on HFD. Results are mean ± SEM (n = 7–11).
*p < 0.05, **p < 0.01, ***p < 0.001. See also Figure S3.

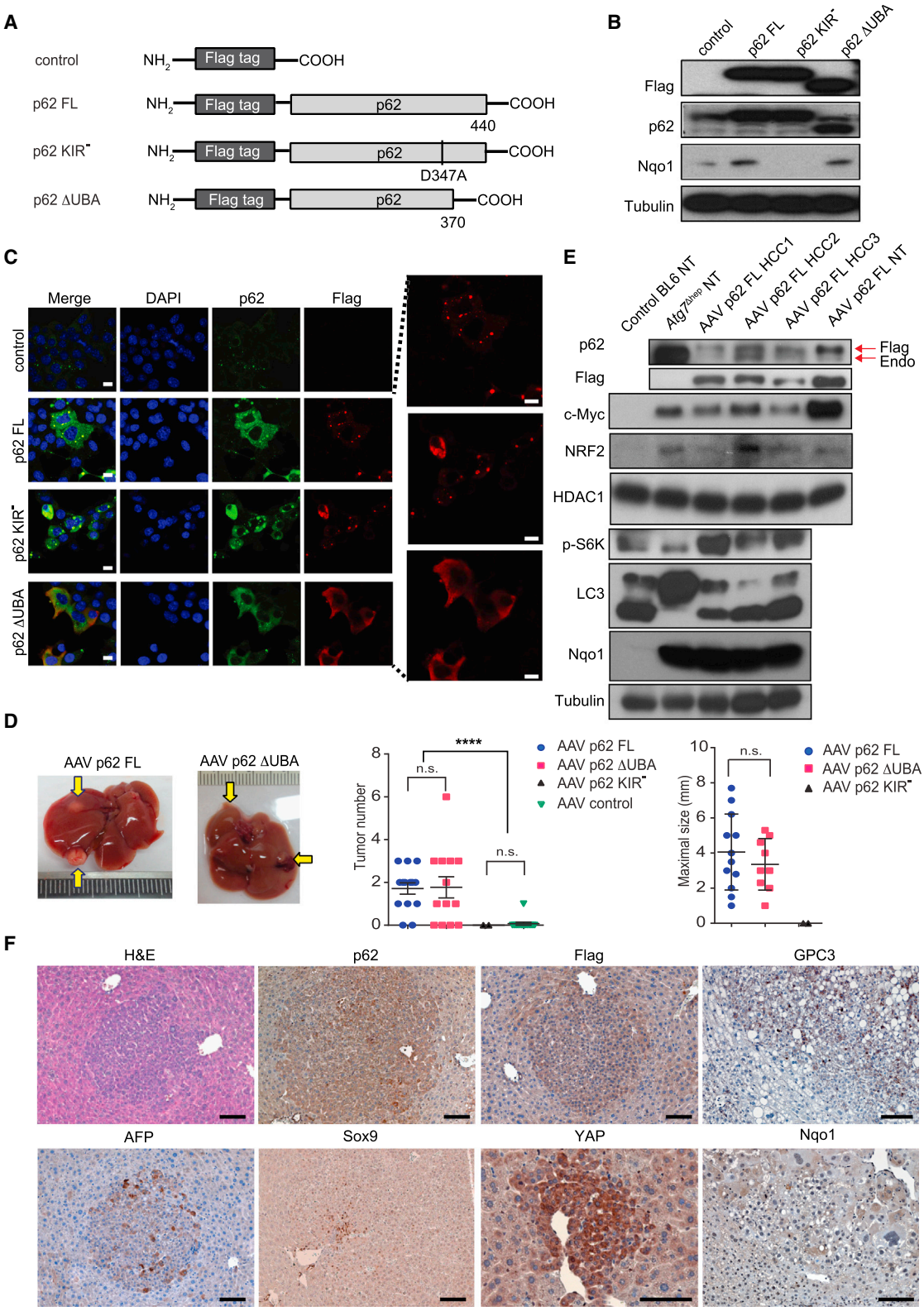

Figure 4. Ectopic p62 Expression Induces HCC

(A) Schematic representation of p62 constructs (FL, full-length p62; KIR^{-}, KIR mutated p62; ΔUBA, UBA-deleted p62; control, FLAG only).

(B) IB analysis of FLAG, p62, and Nqo1 in murine hepatocytes transfected with plasmid expressing p62 or its variants (n = 3).

(legend continued on next page)

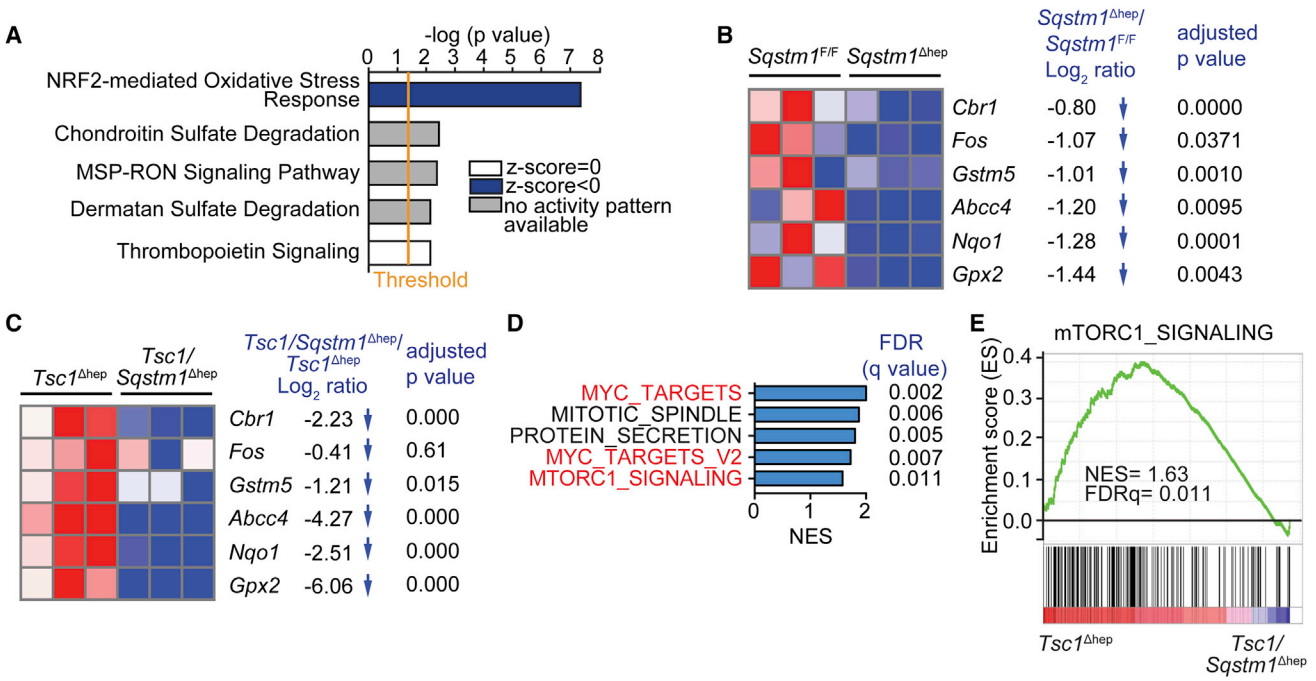

Figure 5. p62-Dependence of the NRF2-Induced Antioxidant Response and mTORC1 Signaling

(A) Ingenuity pathway analysis of genes differentially represented in RNA-seq data from *Sqstm1*$^{\Delta hep}$ versus *Sqstm1*$^{F/F}$ livers (n = 3). Top canonical pathways are ranked by –log (p value) with threshold p value = 0.05. Highest-ranking categories are displayed along the x axis in a decreased order of significance. Blue bars, pathways with *Z* score < 0 (downregulated pathways); gray bars, no activity pattern available; white bars, *Z* score = 0.

(B) Heatmap representation of downregulated genes in *Sqstm1*$^{\Delta hep}$ relative to *Sqstm1*$^{F/F}$ livers (n = 3) associated with "NRF2-mediated Oxidative Stress Response" including Log_2FC and adjusted p value.

(C) Heatmap representation of downregulated genes in *Tsc1/Sqstm1*$^{\Delta hep}$ relative to *Tsc1*$^{\Delta hep}$ livers (n = 3) including Log_2FC and adjusted p value.

(D) GSEA analysis showing that p62 ablation abrogates mTORC1 signaling and reduces expression of c-Myc targets that are induced upon TSC1 ablation. Top five hallmark gene sets sorted by normalized enrichment score comparing *Tsc1/Sqstm1*$^{\Delta hep}$ versus *Tsc1*$^{\Delta hep}$ mice (n = 3). Gene sets related to c-Myc and mTORC1 are colored red.

(E) Enrichment graph of mTORC1_SIGNALING dataset (n = 3).

See also Figure S5.

correlates with p62 and is decreased upon its ablation, results that support earlier findings regarding the ability of p62-mTORC1 signaling to induce c-Myc (Valencia et al., 2014).

Another critical mediator of p62-induced hepatocarcinogenesis is NRF2, whose activation by p62 depends on Keap1 binding. A point mutation in the p62 KIR domain, which prevents Keap1 binding (Suzuki et al., 2013), blocks NRF2 activation and abolishes p62 oncogenic activity. Importantly, NRF2 is mutationally activated in approximately 14% of human HCCs (Schulze et al., 2015; Shibata and Aburatani, 2014). NRF2 is also mutationally activated in chemically induced HCC in rats, where *Nfe2l2* or *Keap1* mutations occur in 70% of early lesions (Zavattari et al., 2015). Given the dependence of NRF2 activation on p62 in the models we studied, the main driver of NRF2 activation in mouse HCC and human HepG2 cells is p62 rather than mutations. Furthermore, no *NRF2* or *KEAP1* mutations were observed in human dysplastic lesions (Nault et al., 2014). NRF2 ablation in *Atg5*$^{\Delta hep}$ mice inhibits the development of adenomas (Ni et al., 2014), but these are benign tumors that emerge in autophagy-deficient livers and their relationship to HCC is questionable.

NRF2 activation and upregulation of its targets are common in human and rodent HCCs, where they occur in the majority of FAH/dysplastic lesions (Farber, 1990; Hayes and McMahon, 2006). It was proposed, but never proved, that NRF2 activation and consequent induction of antioxidant and detoxifying enzymes allow these lesions to survive in chronically stressed livers, where ROS accumulation is readily detected (Nakagawa et al., 2014; Sakurai et al., 2008). Curiously, however, chronic

(C) Expression patterns of p62 constructs in mouse hepatocytes analyzed by IF microscopy (left: blue, DAPI; green, p62; red, FLAG; scale bars, 10 μm). Right: higher magnification of FLAG-positive aggregates. Representative images of three independent experiments are shown.

(D) Representative images of tumor-bearing livers from 12-month-old mice infected with indicated AAV8 vectors. Yellow arrows point to tumors. Tumor numbers and maximal sizes are shown to the right. p62 FL (n = 14); p62 ΔUBA p62 (n = 13); p62 KIR^{-} (n =5 mice infected, only two of which were of the same BL6 genotype as other mice in this figure); control (n = 14). Data are mean ± SEM. n.s., not significant. ****p < 0.0001.

(E) IB analysis of lysates from BL6 and *Atg7*$^{\Delta hep}$ livers, three p62-induced HCCs, and p62 FL infected mouse hepatocytes. (NT). Endo, endogenous p62.

(F) Immunohistochemistry analysis of p62-induced HCCs (n = 10). Scale bars, 100 μm.

See also Figure S4.

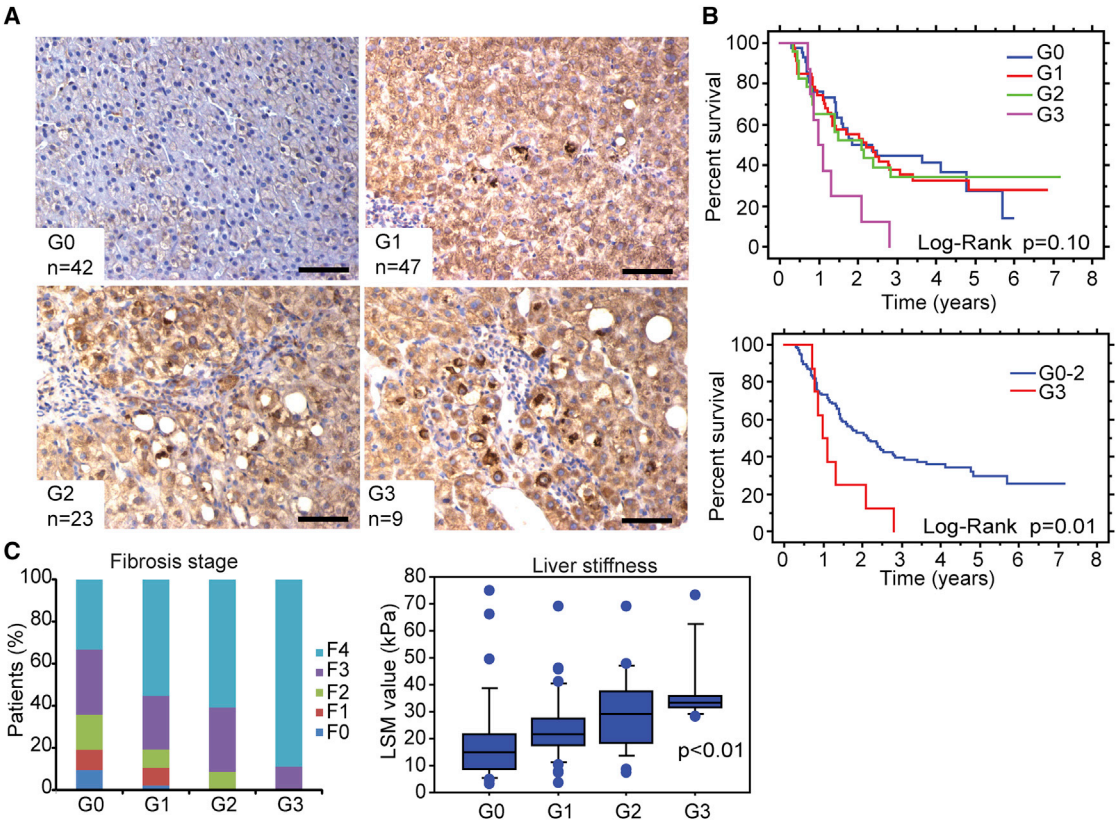

Figure 6. p62-Positive Aggregates in Human Livers Correlate with HCC Recurrence after Curative Ablation

(A) Representative images of p62 immunohistochemistry of non-tumor liver biopsies from human patients with resectable HCC. Biopsies were collected when HCCs were treated curatively. Staining patterns were categorized into four grades (G0–G3) based on number of p62-positive aggregates. Scale bars, 100 μm.

(B) Disease-free survival curves of all four groups (upper panel) and G0–G2 versus G3 groups (lower panel).

(C) Correlation between p62 expression and fibrotic changes in background liver from HCC patients in (B) were analyzed by histological assessment (left panel) and fibroscan (right panel). Box-and-whisker plots showing median (horizontal line), interquartile range (box), and 10th–90th percentiles (whiskers) of the data. Dots indicate outliers. Data of liver stiffness (right panel) were not available in some patients. G0 (n = 32), G1 (n = 41), G2 (n = 22), and G3 (n = 8).

See also Figure S6.

upregulation of these protective enzymes does not inhibit ROS-mediated mutagenesis, as human HCCs contain multiple mutations in addition to those that activate NRF2. On the contrary, persistent NRF2 activation promotes survival of HcPC and allows them to accumulate additional mutations. Congruent with this notion, we find that p62 is required for survival of hepatocytes that accumulate high amounts of superoxides and stain positively with DHE. Although p62 ablation reduces expression of antioxidant enzymes, it decreases rather than increases the number of DHE-positive, ROS-containing cells. Most likely, without NRF2-dependent defenses cells undergoing extensive ROS accumulation die and cannot serve as HCC progenitors. Although exogenous p62 may function by inducing endogenous p62, both this function and activation of the antioxidant response require a functional KIR domain. NRF2 was suggested to induce metabolic reprogramming that favors cell proliferation (DeNicola et al., 2015; Mitsuishi et al., 2012). However, this effect was mainly detected in cancer cell lines that exhibit sustained AKT activation, which is certainly not the case in livers of *Tsc1*$^{\Delta hep}$ or HFD-fed MUP-uPA and STZ-HFD mice, in which AKT is not activated due to hepatic insulin resistance.

Nonetheless, constitutive activation of liver NRF2 does not induce HCC (Kohler et al., 2014). It is plausible that NRF2 only increases HCC risk in the presence of activated mTORC1, as occurs in *Tsc1*$^{\Delta hep}$ livers and during NASH-driven HCC development. Although NRF2 induces *Sqstm1* transcription and p62 activates NRF2 (Figure 7), the latter effect requires p62 phosphorylation by mTORC1 (Ichimura et al., 2013). Future experiments should examine the role of this phosphorylation event in p62-induced tumorigenesis. The ability of p62 to oligomerize and aggregate ubiquitinated proteins was suggested to promote tumorigenesis by inducing oxidative stress (Mathew et al., 2009), and p62 ablation in *Atg7*$^{\Delta hep}$ liver was reported to reduce oxidative stress (Komatsu et al., 2007), results that are not entirely consistent with our current understanding of p62 importance in maintaining liver antioxidant defenses.

Our results illustrate the existence of a common pathway through which diverse etiological factors, including HBV and HCV infections, NASH, and ASH trigger premalignant changes that progress to HCC by inducing p62 accumulation and subsequent NRF2, mTORC1, and c-Myc activation. The

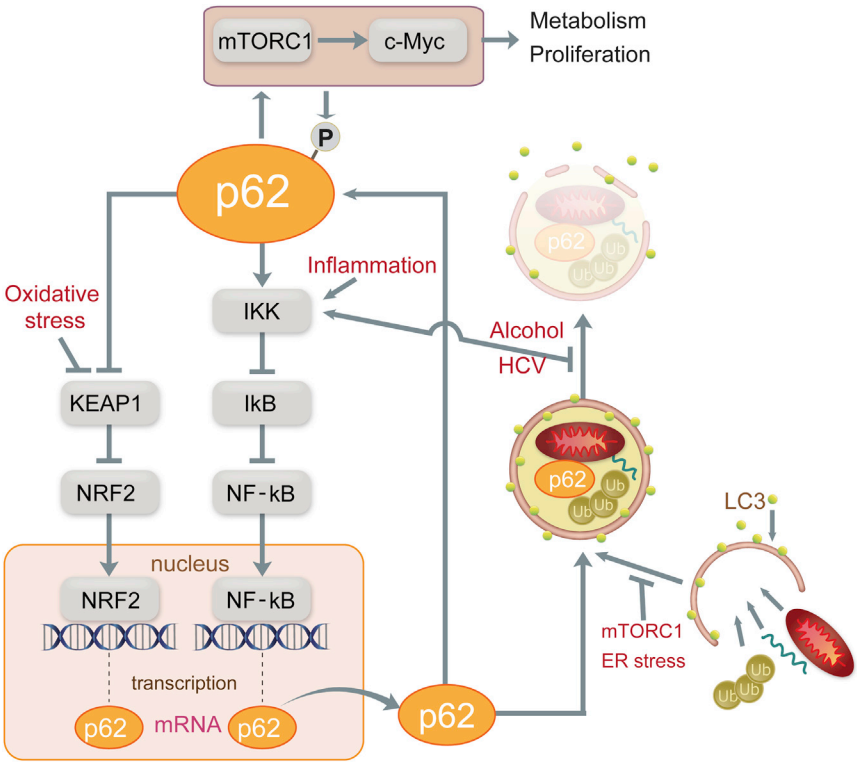

Figure 7. p62 Expression and Signaling during HCC Development

p62 gene transcription is induced by NRF2 and NF-κB, which are activated by oxidative stress and inflammation, respectively. Newly synthesized p62 protein binds ubiquitinated proteins and organelles and LC3 on phagophore membranes to promote autophagy and lysosomal degradation. mTORC1 activation and ER stress promote p62 accumulation by interfering with initiation of autophagy, whereas alcohol and HCV affect p62 by interfering with termination of autophagy and can also lead to IκB kinase (IKK)/NF-κB activation. Once p62 accumulates it leads to IKK/NF-κB activation via TRAF6 binding and NRF2 activation through titration of Keap1. p62 accumulation also activates mTORC1/c-Myc signaling to alter metabolism and promote proliferation. mTORC1-mediated p62 phosphorylation enhances NRF2 activation. P, phosphorylation; Ub, ubiquitination.

p62-Keap1-NRF2 pathway allows HcPC with high ROS content to survive in the chronically stressed liver environment and accumulate numerous mutations that commit them to the malignant fate under conditions where the metabolic and proliferative functions of mTORC1 and c-Myc are also activated. Elevated p62 in human liver predicts rapid recurrence of resectable HCC. Thus, small molecules that interfere with p62 binding to Keap1 and/or TRAF6, which is needed for mTORC1 activation, may be useful for preventing progression of chronic liver disease to HCC as well as attenuate recurrence of resectable HCC.

EXPERIMENTAL PROCEDURES

Mice

Sqstm1$^{F/F}$ and *Tsc1*$^{F/F}$ mice (Mori et al., 2009; Muller et al., 2013) were backcrossed to C57BL/6 mice for at least seven generations and then bred with *Alb-Cre* mice (also C57BL/6) to generate *Sqstm1*$^{F/F}$;*Alb-Cre* (*Sqstm1*$^{\Delta hep}$) and *Tsc1*$^{F/F}$;*Alb-Cre* (*Tsc1*$^{\Delta hep}$) mice, respectively. *Sqstm1*$^{\Delta hep}$ mice were crossed to *Tsc1*$^{\Delta hep}$ and MUP-uPA mice to generate *Tsc1*/*Sqstm1*$^{\Delta hep}$ and *Sqstm1*$^{\Delta hep}$/MUP mice, respectively. All studies used male mice, and were in accordance with NIH guidelines and approved by the UCSD Institutional Animal Care and Use Committee under Dr. Karin's Animal Protocol S00218. Mice were maintained in filter-topped cages on autoclaved chow diet (low-fat diet [LFD], composed of 12% fat, 23% protein, 65% carbohydrates based on caloric content) or HFD, composed of 59% fat, 15% protein, and 26% carbohydrates based on caloric content) (Bio-Serv) and water.

Human Liver Samples

Human tissue specimens were retrospectively obtained from liver biopsies or liver resections, and fixed in buffered formalin and embedded in paraffin using standard methods. Corresponding clinical data were obtained from medical records and de-identified. The study was approved by the institutional review board and research and development committees of the University of Tokyo and Kyoto Prefectural University of Medicine.

ACCESSION NUMBERS

The GEO accession number for RNA-seq data reported in this paper is GEO: GSE77323.

SUPPLEMENTAL INFORMATION

Supplemental Information includes Supplemental Experimental Procedures and six figures and can be found with this article online at http://dx.doi.org/10.1016/j.ccell.2016.04.006.

AUTHOR CONTRIBUTIONS

A.U. designed and performed the main experiments and wrote the paper with M.K., who conceived and supervised the project. F.H., K.T., S.Y., J.F.-B., Z.Z, S.S., S.R., A.D., M.R.-C., S.U., and K.Y. provided technical assistance for the main experiments. A.U., H.N., and K.Y. analyzed human specimens. J.F.-B. and J.F.L. generated p62 mutants. E.S., K.K., and Y.I. discussed and interpreted the results. M.T.D.-M. and J.M. discussed and interpreted the results, analyzed DEN-injected mice, RNA-seq data, and HCC datasets, provided *Sqstm1*$^{F/F}$ mice, and revised the manuscript. M.A.V. provided pathological diagnosis.

ACKNOWLEDGMENTS

We thank E.P. Sandgren and K.L. Guan for MUP-uPA and *Tsc1*$^{F/F}$ mice, respectively, X. Xiao for the AAV vector, H. Nakai and A. Miyanohara for advice and AAV generation, R. Loomba, D.E. Kleiner, T. Kisseleva, and D.A. Brenner for suggestions and constructive criticism, Karin laboratory members for helpful discussions, and Cell Signaling Technology, Santa Cruz Biotechnology, and Abcam for antibodies. A.U., H.N., K.Y., and Y.I. were supported by JSPS KAKENHI Grant (#15H06547, A.U.; #15K19313, H.N.; #25461005, K.Y.; #15K09018, Y.I.), the Kanae Foundation for the Promotion of Medical Science (A.U., H.N.), and a Global Grant Scholarship from The Rotary Foundation (A.U.), the Japanese Society of Gastroenterology (H.N.), and Research

Program on Hepatitis from the Japan Agency for Medical Research and Development, AMED (H.N., K.K.). K.T., J.F.-B., and Z.Z. were supported by Postdoctoral Fellowship for Research Abroad, Research Fellowship for Young Scientists from the JSPS, and a Uehara Memorial Foundation Fellowship (K.T.); CIRM Training Grant II (TG2-01154; J.F.-B.) and Cancer Research Institute (CRI) Irvington postdoctoral fellowship (Z.Z.). M.K. holds the Ben and Wanda Hildyard Chair for Mitochondrial and Metabolic Diseases. Research was supported by the NIH (R01CA163798, R01CA118165, and P01DK098108 to M.K.; R01CA172025 and R01DK108743 to J.M.; R01CA192642 to M.T.D.-M.; 5P30CA030199 to M.T.D.-M. and J.M.), the Superfund Basic Research Program (P42ES010337 to M.K. and E.S.), and the American Association for Study of Liver Diseases/American Liver Foundation (E.S.).

Received: December 10, 2015
Revised: February 1, 2016
Accepted: April 18, 2016
Published: May 19, 2016

REFERENCES

Chandler, R.J., LaFave, M.C., Varshney, G.K., Trivedi, N.S., Carrillo-Carrasco, N., Senac, J.S., Wu, W., Hoffmann, V., Elkahloun, A.G., Burgess, S.M., et al. (2015). Vector design influences hepatic genotoxicity after adeno-associated virus gene therapy. J. Clin. Invest. *125*, 870–880.

Czaja, M.J. (2011). Functions of autophagy in hepatic and pancreatic physiology and disease. Gastroenterology *140*, 1895–1908.

DeNicola, G.M., Chen, P.H., Mullarky, E., Sudderth, J.A., Hu, Z., Wu, D., Tang, H., Xie, Y., Asara, J.M., Huffman, K.E., et al. (2015). NRF2 regulates serine biosynthesis in non-small cell lung cancer. Nat. Genet. *47*, 1475–1481.

Denk, H., Stumptner, C., Fuchsbichler, A., Muller, T., Farr, G., Muller, W., Terracciano, L., and Zatloukal, K. (2006). Are the Mallory bodies and intracellular hyaline bodies in neoplastic and non-neoplastic hepatocytes related? J. Pathol. *208*, 653–661.

Duran, A., Amanchy, R., Linares, J.F., Joshi, J., Abu-Baker, S., Porollo, A., Hansen, M., Moscat, J., and Diaz-Meco, M.T. (2011). p62 is a key regulator of nutrient sensing in the mTORC1 pathway. Mol. Cell *44*, 134–146.

El-Serag, H.B. (2011). Hepatocellular carcinoma. N. Engl. J. Med. *365*, 1118–1127.

Farber, E. (1990). Clonal adaptation during carcinogenesis. Biochem. Pharmacol. *39*, 1837–1846.

Finkin, S., Yuan, D., Stein, I., Taniguchi, K., Weber, A., Unger, K., Browning, J.L., Goossens, N., Nakagawa, S., Gunasekaran, G., et al. (2015). Ectopic lymphoid structures function as microniches for tumor progenitor cells in hepatocellular carcinoma. Nat. Immunol. *16*, 1235–1244.

Font-Burgada, J., Shalapour, S., Ramaswamy, S., Hsueh, B., Rossell, D., Umemura, A., Taniguchi, K., Nakagawa, H., Valasek, M.A., Ye, L., et al. (2015). Hybrid periportal hepatocytes regenerate the injured liver without giving rise to cancer. Cell *162*, 766–779.

Grivennikov, S.I., Greten, F.R., and Karin, M. (2010). Immunity, inflammation, and cancer. Cell *140*, 883–899.

Guichard, C., Amaddeo, G., Imbeaud, S., Ladeiro, Y., Pelletier, L., Maad, I.B., Calderaro, J., Bioulac-Sage, P., Letexier, M., Degos, F., et al. (2012). Integrated analysis of somatic mutations and focal copy-number changes identifies key genes and pathways in hepatocellular carcinoma. Nat. Genet. *44*, 694–698.

Hay, N., and Sonenberg, N. (2004). Upstream and downstream of mTOR. Genes Dev. *18*, 1926–1945.

Hayes, J.D., and McMahon, M. (2006). The double-edged sword of Nrf2: subversion of redox homeostasis during the evolution of cancer. Mol. Cell *21*, 732–734.

Hayes, J.D., and McMahon, M. (2009). NRF2 and KEAP1 mutations: permanent activation of an adaptive response in cancer. Trends Biochem. Sci. *34*, 176–188.

He, G., Dhar, D., Nakagawa, H., Font-Burgada, J., Ogata, H., Jiang, Y., Shalapour, S., Seki, E., Yost, S.E., Jepsen, K., et al. (2013). Identification of liver cancer progenitors whose malignant progression depends on autocrine IL-6 signaling. Cell *155*, 384–396.

Ichimura, Y., Waguri, S., Sou, Y.S., Kageyama, S., Hasegawa, J., Ishimura, R., Saito, T., Yang, Y., Kouno, T., Fukutomi, T., et al. (2013). Phosphorylation of p62 activates the Keap1-Nrf2 pathway during selective autophagy. Mol. Cell *51*, 618–631.

Inami, Y., Waguri, S., Sakamoto, A., Kouno, T., Nakada, K., Hino, O., Watanabe, S., Ando, J., Iwadate, M., Yamamoto, M., et al. (2011). Persistent activation of Nrf2 through p62 in hepatocellular carcinoma cells. J. Cell Biol. *193*, 275–284.

Iwadate, R., Inoue, J., Tsuda, H., Takano, M., Furuya, K., Hirasawa, A., Aoki, D., and Inazawa, J. (2015). High expression of p62 protein is associated with poor prognosis and aggressive phenotypes in endometrial cancer. Am. J. Pathol. *185*, 2523–2533.

Jain, A., Lamark, T., Sjottem, E., Larsen, K.B., Awuh, J.A., Overvatn, A., McMahon, M., Hayes, J.D., and Johansen, T. (2010). p62/SQSTM1 is a target gene for transcription factor NRF2 and creates a positive feedback loop by inducing antioxidant response element-driven gene transcription. J. Biol. Chem. *285*, 22576–22591.

Kang, J.S., Wanibuchi, H., Morimura, K., Gonzalez, F.J., and Fukushima, S. (2007). Role of CYP2E1 in diethylnitrosamine-induced hepatocarcinogenesis in vivo. Cancer Res. *67*, 11141–11146.

Kaposi-Novak, P., Libbrecht, L., Woo, H.G., Lee, Y.H., Sears, N.C., Coulouarn, C., Conner, E.A., Factor, V.M., Roskams, T., and Thorgeirsson, S.S. (2009). Central role of c-Myc during malignant conversion in human hepatocarcinogenesis. Cancer Res. *69*, 2775–2782.

Kawai, D., Takaki, A., Nakatsuka, A., Wada, J., Tamaki, N., Yasunaka, T., Koike, K., Tsuzaki, R., Matsumoto, K., Miyake, Y., et al. (2012). Hydrogen-rich water prevents progression of nonalcoholic steatohepatitis and accompanying hepatocarcinogenesis in mice. Hepatology *56*, 912–921.

Kim, Y.R., Oh, J.E., Kim, M.S., Kang, M.R., Park, S.W., Han, J.Y., Eom, H.S., Yoo, N.J., and Lee, S.H. (2010). Oncogenic NRF2 mutations in squamous cell carcinomas of oesophagus and skin. J. Pathol. *220*, 446–451.

Kohler, U.A., Kurinna, S., Schwitter, D., Marti, A., Schafer, M., Hellerbrand, C., Speicher, T., and Werner, S. (2014). Activated Nrf2 impairs liver regeneration in mice by activation of genes involved in cell-cycle control and apoptosis. Hepatology *60*, 670–678.

Komatsu, M., Waguri, S., Koike, M., Sou, Y.S., Ueno, T., Hara, T., Mizushima, N., Iwata, J., Ezaki, J., Murata, S., et al. (2007). Homeostatic levels of p62 control cytoplasmic inclusion body formation in autophagy-deficient mice. Cell *131*, 1149–1163.

Komatsu, M., Kageyama, S., and Ichimura, Y. (2012). p62/SQSTM1/A170: physiology and pathology. Pharmacol. Res. *66*, 457–462.

Kuraishy, A., Karin, M., and Grivennikov, S.I. (2011). Tumor promotion via injury- and death-induced inflammation. Immunity *35*, 467–477.

Li, L., Shen, C., Nakamura, E., Ando, K., Signoretti, S., Beroukhim, R., Cowley, G.S., Lizotte, P., Liberzon, E., Bair, S., et al. (2013). SQSTM1 is a pathogenic target of 5q copy number gains in kidney cancer. Cancer Cell *24*, 738–750.

Linares, J.F., Duran, A., Yajima, T., Pasparakis, M., Moscat, J., and Diaz-Meco, M.T. (2013). K63 polyubiquitination and activation of mTOR by the p62-TRAF6 complex in nutrient-activated cells. Mol. Cell *51*, 283–296.

Linares, J.F., Duran, A., Reina-Campos, M., Aza-Blanc, P., Campos, A., Moscat, J., and Diaz-Meco, M.T. (2015). Amino acid activation of mTORC1 by a PB1-domain-driven kinase complex cascade. Cell Rep. *12*, 1339–1352.

Ling, J., Kang, Y., Zhao, R., Xia, Q., Lee, D.F., Chang, Z., Li, J., Peng, B., Fleming, J.B., Wang, H., et al. (2012). KrasG12D-induced IKK2/beta/NF-kappaB activation by IL-1alpha and p62 feedforward loops is required for development of pancreatic ductal adenocarcinoma. Cancer Cell *21*, 105–120.

Luch, A. (2005). Nature and nurture - lessons from chemical carcinogenesis. Nat. Rev. Cancer *5*, 113–125.

Maeda, S., Kamata, H., Luo, J.L., Leffert, H., and Karin, M. (2005). IKKbeta couples hepatocyte death to cytokine-driven compensatory proliferation that promotes chemical hepatocarcinogenesis. Cell *121*, 977–990.

Malhi, H., and Kaufman, R.J. (2011). Endoplasmic reticulum stress in liver disease. J. Hepatol. *54*, 795–809.

Mathew, R., Karp, C.M., Beaudoin, B., Vuong, N., Chen, G., Chen, H.Y., Bray, K., Reddy, A., Bhanot, G., Gelinas, C., et al. (2009). Autophagy suppresses tumorigenesis through elimination of p62. Cell *137*, 1062–1075.

Menon, S., Yecies, J.L., Zhang, H.H., Howell, J.J., Nicholatos, J., Harputlugil, E., Bronson, R.T., Kwiatkowski, D.J., and Manning, B.D. (2012). Chronic activation of mTOR complex 1 is sufficient to cause hepatocellular carcinoma in mice. Sci. Signal. *5*, ra24.

Min, L., Ji, Y., Bakiri, L., Qiu, Z., Cen, J., Chen, X., Chen, L., Scheuch, H., Zheng, H., Qin, L., et al. (2012). Liver cancer initiation is controlled by AP-1 through SIRT6-dependent inhibition of survivin. Nat. Cell Biol. *14*, 1203–1211.

Mitsuishi, Y., Taguchi, K., Kawatani, Y., Shibata, T., Nukiwa, T., Aburatani, H., Yamamoto, M., and Motohashi, H. (2012). Nrf2 redirects glucose and glutamine into anabolic pathways in metabolic reprogramming. Cancer Cell *22*, 66–79.

Mori, H., Inoki, K., Munzberg, H., Opland, D., Faouzi, M., Villanueva, E.C., Ikenoue, T., Kwiatkowski, D., MacDougald, O.A., Myers, M.G., Jr., et al. (2009). Critical role for hypothalamic mTOR activity in energy balance. Cell Metab. *9*, 362–374.

Muller, T.D., Lee, S.J., Jastroch, M., Kabra, D., Stemmer, K., Aichler, M., Abplanalp, B., Ananthakrishnan, G., Bhardwaj, N., Collins, S., et al. (2013). p62 links beta-adrenergic input to mitochondrial function and thermogenesis. J. Clin. Invest. *123*, 469–478.

Nakagawa, H., Umemura, A., Taniguchi, K., Font-Burgada, J., Dhar, D., Ogata, H., Zhong, Z., Valasek, M.A., Seki, E., Hidalgo, J., et al. (2014). ER stress cooperates with hypernutrition to trigger TNF-dependent spontaneous HCC development. Cancer Cell *26*, 331–343.

Nault, J.C., Calderaro, J., Di Tommaso, L., Balabaud, C., Zafrani, E.S., Bioulac-Sage, P., Roncalli, M., and Zucman-Rossi, J. (2014). Telomerase reverse transcriptase promoter mutation is an early somatic genetic alteration in the transformation of premalignant nodules in hepatocellular carcinoma on cirrhosis. Hepatology *60*, 1983–1992.

Ni, H.M., Woolbright, B.L., Williams, J., Copple, B., Cui, W., Luyendyk, J.P., Jaeschke, H., and Ding, W.X. (2014). Nrf2 promotes the development of fibrosis and tumorigenesis in mice with defective hepatic autophagy. J. Hepatol. *61*, 617–625.

Ohta, T., Iijima, K., Miyamoto, M., Nakahara, I., Tanaka, H., Ohtsuji, M., Suzuki, T., Kobayashi, A., Yokota, J., Sakiyama, T., et al. (2008). Loss of Keap1 function activates Nrf2 and provides advantages for lung cancer cell growth. Cancer Res. *68*, 1303–1309.

Park, E.J., Lee, J.H., Yu, G.Y., He, G., Ali, S.R., Holzer, R.G., Osterreicher, C.H., Takahashi, H., and Karin, M. (2010). Dietary and genetic obesity promote liver inflammation and tumorigenesis by enhancing IL-6 and TNF expression. Cell *140*, 197–208.

Qu, A., Jiang, C., Cai, Y., Kim, J.H., Tanaka, N., Ward, J.M., Shah, Y.M., and Gonzalez, F.J. (2014). Role of Myc in hepatocellular proliferation and hepatocarcinogenesis. J. Hepatol. *60*, 331–338.

Rubin, H. (2011). Fields and field cancerization: the preneoplastic origins of cancer: asymptomatic hyperplastic fields are precursors of neoplasia, and their progression to tumors can be tracked by saturation density in culture. Bioessays *33*, 224–231.

Sakurai, T., Maeda, S., Chang, L., and Karin, M. (2006). Loss of hepatic NF-kappa B activity enhances chemical hepatocarcinogenesis through sustained c-Jun N-terminal kinase 1 activation. Proc. Natl. Acad. Sci. USA *103*, 10544–10551.

Sakurai, T., He, G., Matsuzawa, A., Yu, G.Y., Maeda, S., Hardiman, G., and Karin, M. (2008). Hepatocyte necrosis induced by oxidative stress and IL-1 alpha release mediate carcinogen-induced compensatory proliferation and liver tumorigenesis. Cancer Cell *14*, 156–165.

Sanz, L., Diaz-Meco, M.T., Nakano, H., and Moscat, J. (2000). The atypical PKC-interacting protein p62 channels NF-kappaB activation by the IL-1-TRAF6 pathway. EMBO J. *19*, 1576–1586.

Schneider, J.L., and Cuervo, A.M. (2014). Liver autophagy: much more than just taking out the trash. Nat. Rev. Gastroenterol. Hepatol. *11*, 187–200.

Schulze, K., Imbeaud, S., Letouze, E., Alexandrov, L.B., Calderaro, J., Rebouissou, S., Couchy, G., Meiller, C., Shinde, J., Soysouvanh, F., et al. (2015). Exome sequencing of hepatocellular carcinomas identifies new mutational signatures and potential therapeutic targets. Nat. Genet. *47*, 505–511.

Sell, S., and Leffert, H.L. (2008). Liver cancer stem cells. J. Clin. Oncol. *26*, 2800–2805.

Shibata, T., and Aburatani, H. (2014). Exploration of liver cancer genomes. Nat. Rev. Gastroenterol. Hepatol. *11*, 340–349.

Shibata, T., Ohta, T., Tong, K.I., Kokubu, A., Odogawa, R., Tsuta, K., Asamura, H., Yamamoto, M., and Hirohashi, S. (2008). Cancer related mutations in NRF2 impair its recognition by Keap1-Cul3 E3 ligase and promote malignancy. Proc. Natl. Acad. Sci. USA *105*, 13568–13573.

Solinas, G., Naugler, W., Galimi, F., Lee, M.S., and Karin, M. (2006). Saturated fatty acids inhibit induction of insulin gene transcription by JNK-mediated phosphorylation of insulin-receptor substrates. Proc. Natl. Acad. Sci. USA *103*, 16454–16459.

Starley, B.Q., Calcagno, C.J., and Harrison, S.A. (2010). Nonalcoholic fatty liver disease and hepatocellular carcinoma: a weighty connection. Hepatology *51*, 1820–1832.

Suzuki, T., Motohashi, H., and Yamamoto, M. (2013). Toward clinical application of the Keap1-Nrf2 pathway. Trends Pharmacol. Sci. *34*, 340–346.

Takamura, A., Komatsu, M., Hara, T., Sakamoto, A., Kishi, C., Waguri, S., Eishi, Y., Hino, O., Tanaka, K., and Mizushima, N. (2011). Autophagy-deficient mice develop multiple liver tumors. Genes Dev. *25*, 795–800.

Totoki, Y., Tatsuno, K., Covington, K.R., Ueda, H., Creighton, C.J., Kato, M., Tsuji, S., Donehower, L.A., Slagle, B.L., Nakamura, H., et al. (2014). Trans-ancestry mutational landscape of hepatocellular carcinoma genomes. Nat. Genet. *46*, 1267–1273.

Umemura, A., Park, E.J., Taniguchi, K., Lee, J.H., Shalapour, S., Valasek, M.A., Aghajan, M., Nakagawa, H., Seki, E., Hall, M.N., et al. (2014). Liver damage, inflammation, and enhanced tumorigenesis after persistent mTORC1 inhibition. Cell Metab. *20*, 133–144.

Valencia, T., Kim, J.Y., Abu-Baker, S., Moscat-Pardos, J., Ahn, C.S., Reina-Campos, M., Duran, A., Castilla, E.A., Metallo, C.M., Diaz-Meco, M.T., et al. (2014). Metabolic reprogramming of stromal fibroblasts through p62-mTORC1 signaling promotes inflammation and tumorigenesis. Cancer Cell *26*, 121–135.

van de Wetering, M., Francies, H.E., Francis, J.M., Bounova, G., Iorio, F., Pronk, A., van Houdt, W., van Gorp, J., Taylor-Weiner, A., Kester, L., et al. (2015). Prospective derivation of a living organoid biobank of colorectal cancer patients. Cell *161*, 933–945.

Vogelstein, B., Papadopoulos, N., Velculescu, V.E., Zhou, S., Diaz, L.A., Jr., and Kinzler, K.W. (2013). Cancer genome landscapes. Science *339*, 1546–1558.

Wolf, M.J., Adili, A., Piotrowitz, K., Abdullah, Z., Boege, Y., Stemmer, K., Ringelhan, M., Simonavicius, N., Egger, M., Wohlleber, D., et al. (2014). Metabolic activation of intrahepatic CD8+ T cells and NKT cells causes nonalcoholic steatohepatitis and liver cancer via cross-talk with hepatocytes. Cancer Cell *26*, 549–564.

Zatloukal, K., French, S.W., Stumptner, C., Strnad, P., Harada, M., Toivola, D.M., Cadrin, M., and Omary, M.B. (2007). From Mallory to Mallory-Denk bodies: what, how and why? Exp. Cell Res. *313*, 2033–2049.

Zavattari, P., Perra, A., Menegon, S., Kowalik, M.A., Petrelli, A., Angioni, M.M., Follenzi, A., Quagliata, L., Ledda-Columbano, G.M., Terracciano, L., et al. (2015). Nrf2, but not beta-catenin, mutation represents an early event in rat hepatocarcinogenesis. Hepatology *62*, 851–862.

Cancer Cell, Volume *29*

Supplemental Information

p62, Upregulated during Preneoplasia, Induces Hepatocellular Carcinogenesis by Maintaining Survival of Stressed HCC-Initiating Cells

Atsushi Umemura, Feng He, Koji Taniguchi, Hayato Nakagawa, Shinichiro Yamachika, Joan Font-Burgada, Zhenyu Zhong, Shankar Subramaniam, Sindhu Raghunandan, Angeles Duran, Juan F. Linares, Miguel Reina-Campos, Shiori Umemura, Mark A. Valasek, Ekihiro Seki, Kanji Yamaguchi, Kazuhiko Koike, Yoshito Itoh, Maria T. Diaz-Meco, Jorge Moscat, and Michael Karin

Supplemental Data

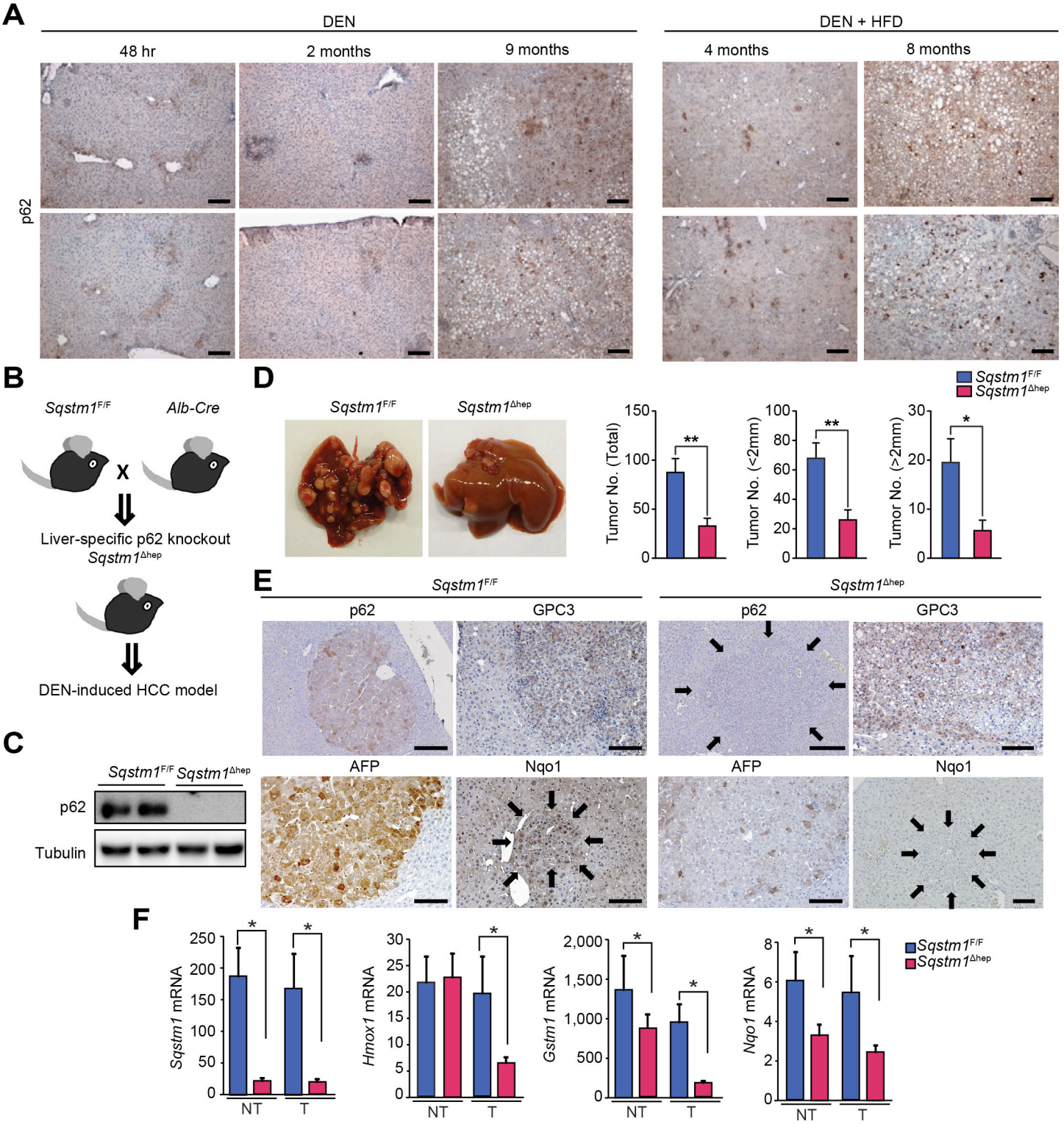

Figure S1, related to Figure 1. p62 ablation attenuates DEN-induced liver carcinogenesis.

(**A**) IHC of p62 in mouse livers after different DEN treatments. DEN 48 hr; mice were injected with DEN (100 mg/kg) at 8 weeks of age and sacrificed 48 hr later. DEN 2, 9 months; mice were injected with DEN (25 mg/kg) at 2 weeks of age and sacrificed 2 or 9 months later. n=3 mice per treatment. DEN + HFD 4, 8 months; mice were injected with DEN (25 mg/kg) at 2 weeks of age and sacrificed 4 or 8 months later. Mice were kept on HFD from 4 weeks after DEN injection until analysis. n=3. (**B**) Scheme for generating liver-specific p62 knock out mice. *Sqstm1*$^{F/F}$ mice were crossed with *Alb-Cre* transgenic mice to generate *Sqstm1*$^{F/F}$*;Alb-Cre (Sqstm1*$^{\Delta hep}$*)* mice. Two week old *Sqstm1*$^{F/F}$ and *Sqstm1*$^{\Delta hep}$ males were injected with 25 mg/kg DEN. Tumor development was analyzed 8 months later. (**C**) p62 and tubulin IB of 8 week old *Sqstm1*$^{F/F}$ and *Sqstm1*$^{\Delta hep}$ mouse liver lysates. (n=4). (**D**) Gross morphology of tumor-bearing livers from *Sqstm1*$^{F/F}$ and *Sqstm1*$^{\Delta hep}$ mice kept on HFD from 4 weeks after DEN injection until analysis (left panel). Numbers of tumors of indicated sizes in livers of *Sqstm1*$^{F/F}$ and *Sqstm1*$^{\Delta hep}$ mice injected with DEN and kept on HFD (right panel). Results are means ± S.D. (n=11-13) (**E**) IHC of liver tumors from *Sqstm1*$^{F/F}$ and *Sqstm1*$^{\Delta hep}$ mice using antibodies to p62, AFP, GPC3, and Nqo1. Arrows indicate tumor portion. (n=4). (**F**) Relative mRNA amount of *Sqstm1* and NRF2 target genes, *Hmox1*, *Gstm1*, and *Nqo1*, in non-tumor (NT) and tumor (T) liver tissue of 8 month old *Sqstm1*$^{F/F}$ and *Sqstm1*$^{\Delta hep}$ mice determined by real time qPCR. Results are means ± S.D. (n = 6). *$p < 0.05$, **$p < 0.01$. Scale bars: 100 μm.

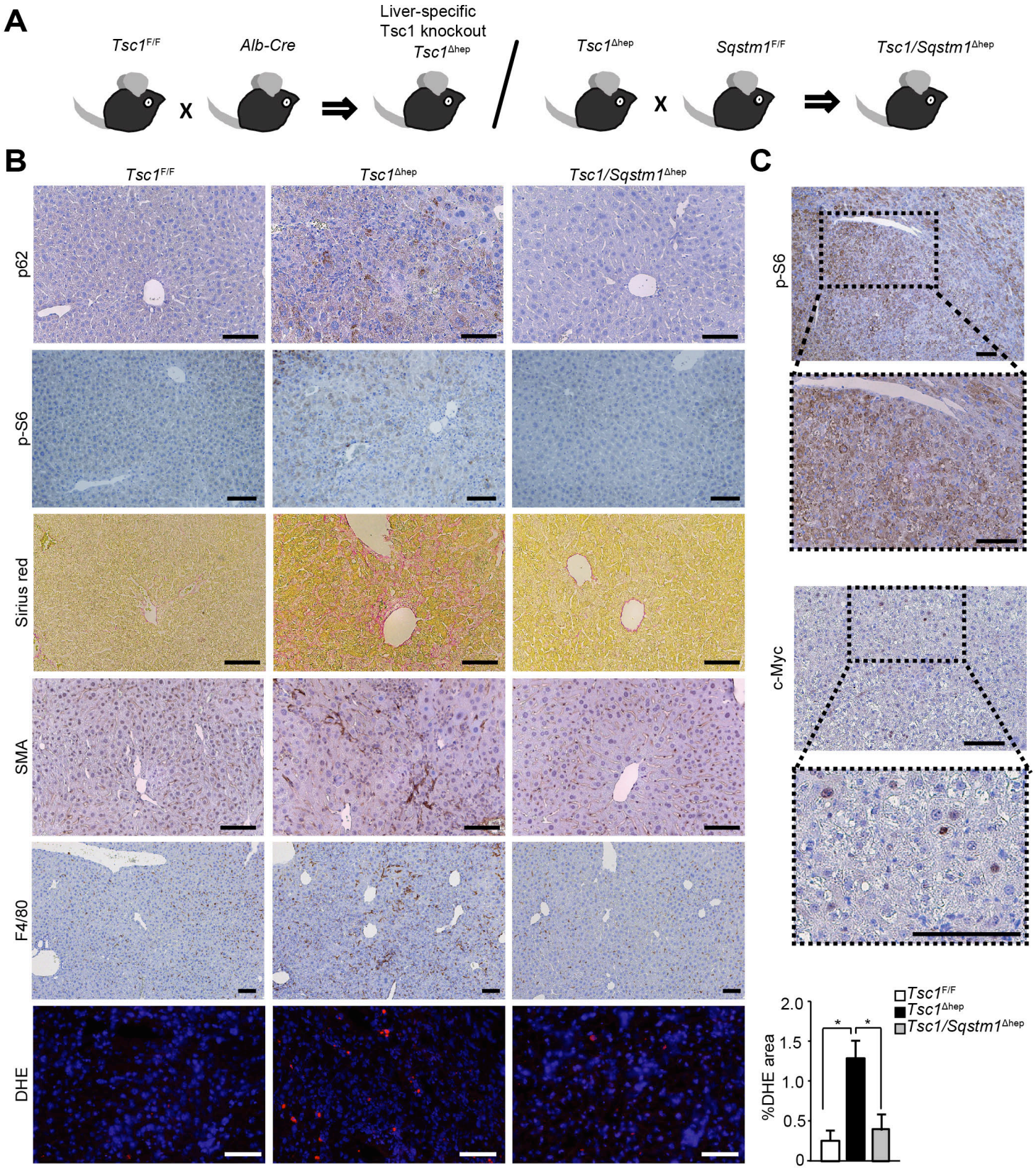
A
Tsc1F/F
Alb-Cre
Liver-specific
Tsc1 knockout
Tsc1Δhep
Tsc1Δhep
Sqstm1F/F
Tsc1/Sqstm1Δhep
B
Tsc1F/F
Tsc1Δhep
Tsc1/Sqstm1Δhep
p62
p-S6
Sirius red
SMA
F4/80
DHE
C
p-S6
c-Myc
%DHE area
2.0
1.5
1.0
0.5
0
*
*
Tsc1F/F
Tsc1Δhep
Tsc1/Sqstm1Δhep

Figure S2, related to Figure 2. Loss of p62 attenuates liver pathology in *Tsc1*$^{\Delta hep}$ mice.

(**A**) Schemes for generation of liver-specific *Tsc1*$^{\Delta hep}$ single knockout, and *Tsc1/Sqstm1*$^{\Delta hep}$ double knockout mice. *Tsc1*$^{\Delta hep}$ mice were obtained in the same way as *Sqstm1*$^{\Delta hep}$. *Tsc1*$^{\Delta hep}$ mice were crossed with *Sqstm1*$^{F/F}$ mice to generate *Tsc1/Sqstm1*$^{\Delta hep}$ mice. (**B**) IHC analysis of p62, phospho-S6, SMA, and F4/80 in liver sections of indicated mouse strains. Liver fibrosis and ROS accumulation were assessed by Sirius red staining and DHE staining, respectively. Results are means ± S.D. (n = 4). (**C**) IHC staining of phospho-S6 and c-Myc in tumor tissue from *Tsc1*$^{\Delta hep}$ mice (n = 3). *$p < 0.05$. Scale bars: 100 μm.

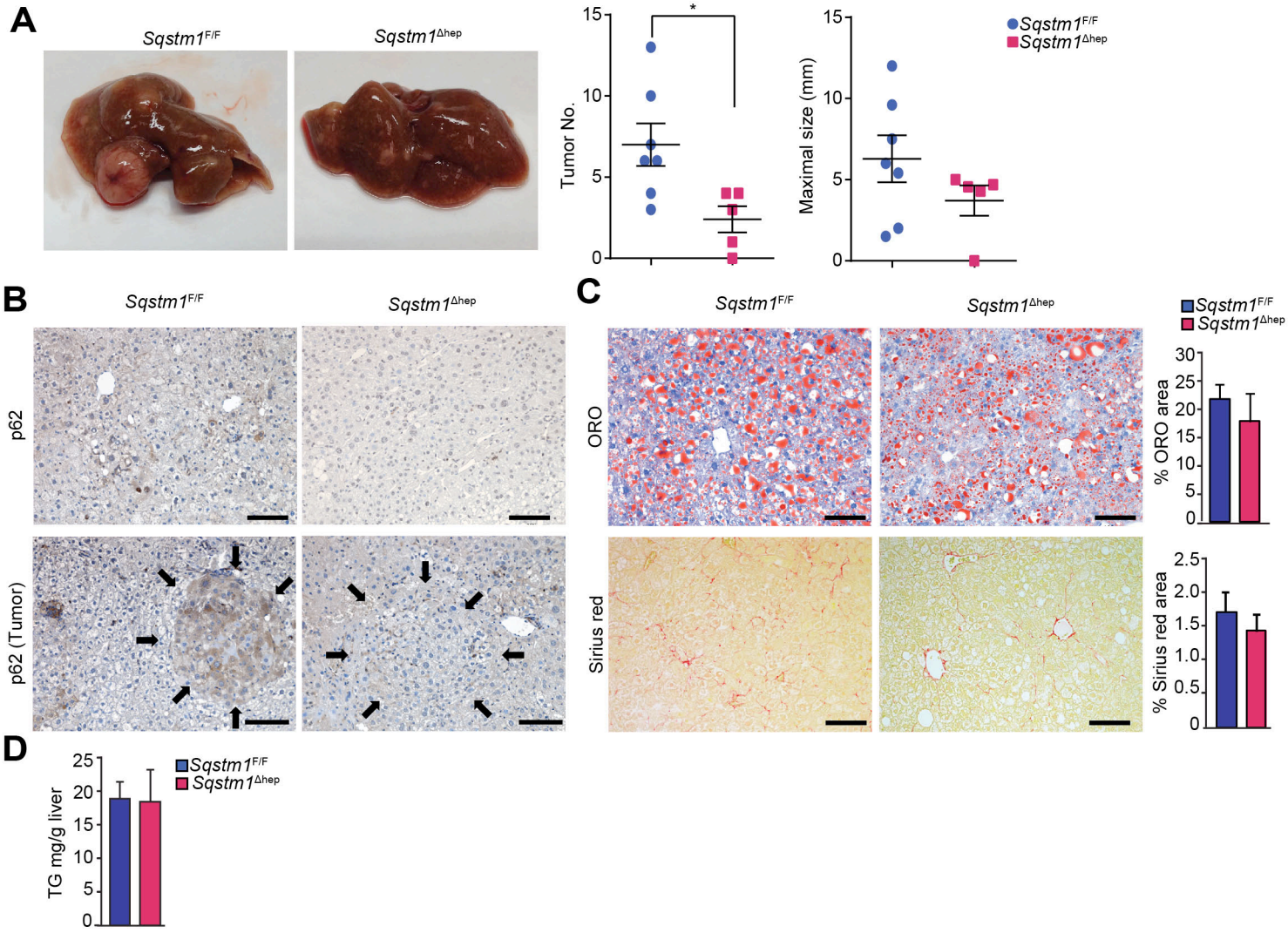

Figure S3, related to Figure 3. Loss of p62 attenuates HCC development but not hepatic steatosis in STZ-HFD mice.

(**A**) Gross morphology of livers bearing tumors (left), and tumor numbers and maximal sizes (right) in 5 months old *Sqstm1*$^{F/F}$ and *Sqstm1*$^{\Delta hep}$ STZ-HFD mice. Results are means ± S.E.M. (n=5-7). (**B, C**) p62 expression, lipid droplets, and fibrosis in non-tumor and tumor portions from livers of 5 months old *Sqstm1*$^{F/F}$ and *Sqstm1*$^{\Delta hep}$ STZ-HFD mice were examined by p62 IHC, Oil Red O (ORO), and Sirius red staining, respectively. Quantitation of areas occupied by stained cells is shown on the right, (n=3). Arrows indicate tumor portion. (**D**) TG content in livers from 5 months old *Sqstm1*$^{F/F}$ and *Sqstm1*$^{\Delta hep}$ STZ-HFD mice. (n=4) Scale bars: 100 μm. *p < 0.05. Results are means ± S.D.

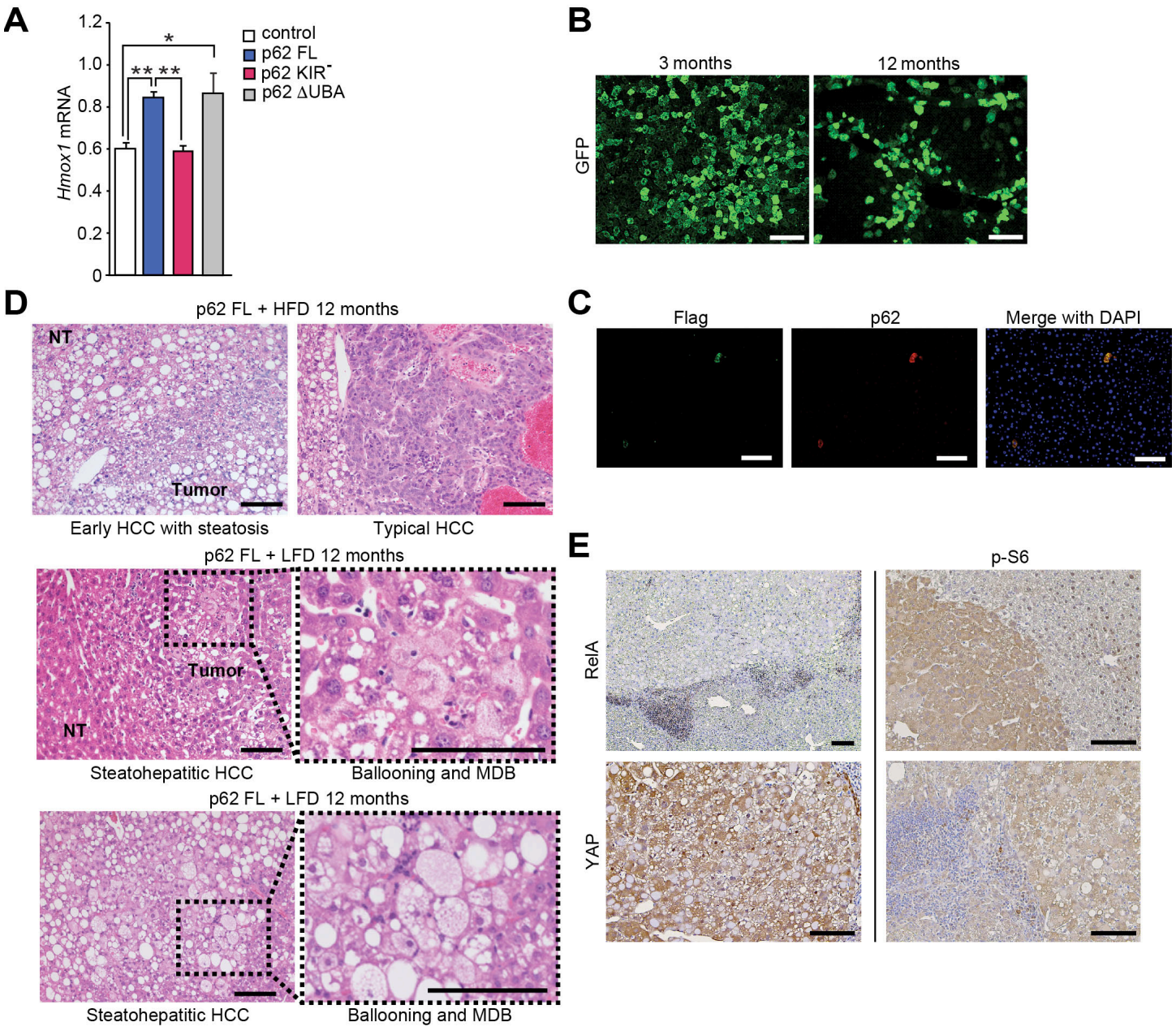

Figure S4, related to Figure 4. Ectopic expression of p62 induces HCC.

(**A**) Relative *Hmox1* mRNA expression in hepatocytes transfected with indicated p62 constructs. Results are normalized to GAPDH as in Figure 2D. Results are means ± S.D. (n=3). (**B**) AAV8-GFP infection efficiency and stability of expression were determined by GFP immunofluorescent staining of livers at the indicated times after infection. (n=3). (**C**) Analysis of Flag and p62 coexpression in AAV8-p62 FL infected mouse hepatocytes. (n=3). (**D**) Histological assessment of p62-induced tumors by H&E staining (NT; non-tumor). (n=10). (**E**) RelA, YAP, and phospho-S6 IHC analysis of p62-induced HCCs. (n=10). *$p < 0.05$, **$p < 0.01$. Scale bars: 100 μm.

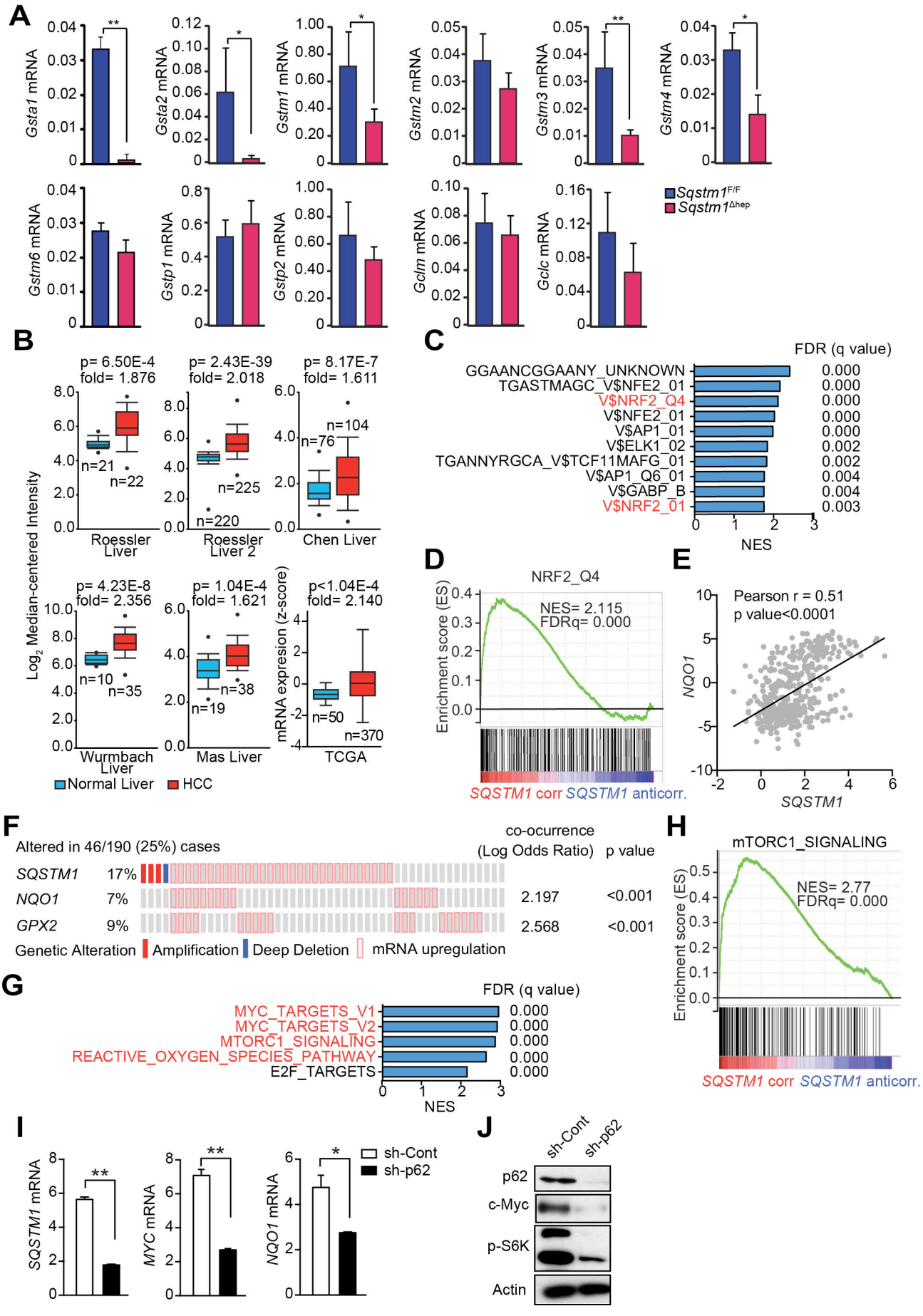
A
Gsta1 mRNA
Gsta2 mRNA
Gstm1 mRNA
Gstm2 mRNA
Gstm3 mRNA
Gstm4 mRNA
Gstm6 mRNA
Gstp1 mRNA
Gstp2 mRNA
Gclm mRNA
Gclc mRNA
Sqstm1F/F
Sqstm1Δhep
B
p= 6.50E-4 fold= 1.876
p= 2.43E-39 fold= 2.018
p= 8.17E-7 fold= 1.611
p= 4.23E-8 fold= 2.356
p= 1.04E-4 fold= 1.621
p<1.04E-4 fold= 2.140
Log2 Median-centered Intensity
mRNA expression (z-score)
n=21
n=22
n=225
n=220
n=104
n=76
n=10
n=35
n=38
n=19
n=50
n=370
Roessler Liver
Roessler Liver 2
Chen Liver
Wurmbach Liver
Mas Liver
TCGA
Normal Liver
HCC
C
FDR (q value)
GGAANCGGAANY_UNKNOWN 0.000
TGASTMAGC_V$NFE2_01 0.000
V$NRF2_Q4 0.000
V$NFE2_01 0.000
V$AP1_01 0.000
V$ELK1_02 0.002
TGANNYRGCA_V$TCF11MAFG_01 0.002
V$AP1_Q6_01 0.004
V$GABP_B 0.004
V$NRF2_01 0.003
NES
D
NRF2_Q4
NES= 2.115
FDRq= 0.000
Enrichment score (ES)
SQSTM1 corr SQSTM1 anticorr.
E
Pearson r = 0.51
p value<0.0001
NQO1
SQSTM1
F
Altered in 46/190 (25%) cases
co-ocurrence (Log Odds Ratio)
p value
SQSTM1 17%
NQO1 7% 2.197 <0.001
GPX2 9% 2.568 <0.001
Genetic Alteration Amplification Deep Deletion mRNA upregulation
G
FDR (q value)
MYC_TARGETS_V1 0.000
MYC_TARGETS_V2 0.000
MTORC1_SIGNALING 0.000
REACTIVE_OXYGEN_SPECIES_PATHWAY 0.000
E2F_TARGETS 0.000
NES
H
mTORC1_SIGNALING
NES= 2.77
FDRq= 0.000
Enrichment score (ES)
SQSTM1 corr SQSTM1 anticorr.
I
SQSTM1 mRNA
MYC mRNA
NQO1 mRNA
sh-Cont
sh-p62
J
sh-Cont
sh-p62
p62
c-Myc
p-S6K
Actin

Figure S5, related to Figure 5. p62 expression correlates with NRF2 and mTORC1 activation in human HCC. (**A**) Relative mRNA amount of NRF2 target genes, *Gsta1*, *Gsta2*, *Gstm1*, *Gstm2*, *Gstm3*, *Gstm4*, *Gstm6*, *Gstp1*, *Gstp2*, *Gclm*, and *Gclc*, in livers of 10 months old *Sqstm1*$^{F/F}$ and *Sqstm1*$^{\Delta hep}$ mice determined by real time qPCR, and results are means ± S.D. (n = 3-5). Results are normalized to GAPDH as in Figure 2D. (**B**) *SQSTM1* mRNA levels in normal human livers and HCCs in different clinical cohorts. Datasets extracted from Oncomine (Roessler, Chen, Wurmbach and Mas Liver) and TCGA. Box-and-whisker plots showing median (horizontal line), interquartile range (box) and 10th-90th percentiles (whiskers) of the data of Oncomine and min to max (whiskers) of the data of TGCA. Dots indicate outliers. (**C**) List of top-ten genesets from C3 compilation (MSigDb) scored for enrichment using GSEA of *SQSTM1* correlation profile in the TCGA dataset (LIVER). Enrichments of NRF2 genesets are highlighted in red. (**D**) Enrichment graph of the NRF2 signature. (**E**) Strong correlation between *SQSTM1* and *NQO1* expression. Correlation analysis including linear regression and Pearson correlation analysis. n=423. (**F**) *SQSTM1* overexpression tends to co-occur with overexpression of *NQO1* and *GPX2*. Oncoprint graph representing alterations in each patient (grey square) within the TCGA dataset available at cBioportal (n=190). Co-occurrence showed as Log Odds ratio between *SQSTM1* and *NQO1* and *GPX2*, respectively. (**G**) List of top-five genesets from Hallmark compilation (MSigDb) scored for enrichment using GSEA of *SQSTM1* correlation profile in the TCGA dataset (LIVER). n=423. In red, genesets related to c-Myc, mTORC1 and ROS. (**H**) Enrichment graph of mTORC1_Signaling. (**I, J**) p62 expression in human HCC cell line, HepG2, was silenced using shRNA (control shRNA; sh-Cont, p62 shRNA; sh-p62). (**I**) *SQSTM1*, *MYC*, and *NQO1* mRNA expressions were quantitated by real time qPCR. Results are means ± S.D. (n = 3). (**J**) p62, c-Myc and S6K phosphorylation were analyzed by immunoblotting (n = 3). *$p < 0.05$, **$p < 0.01$.

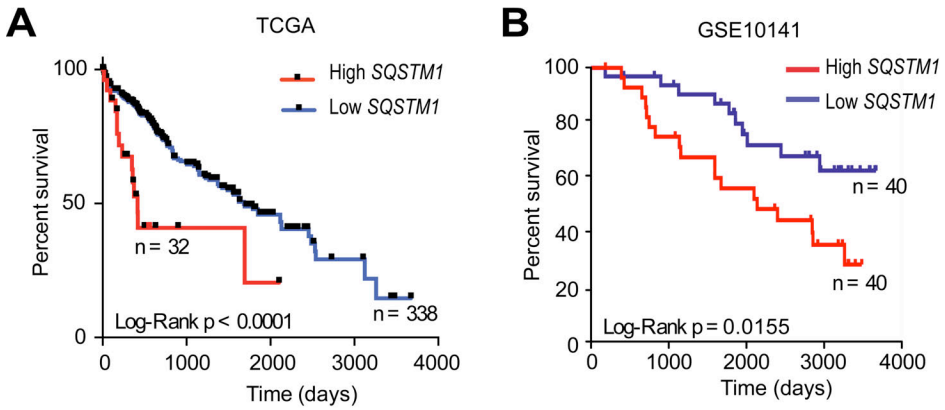

Figure S6, related to Figure 6. HCC survival is p62-dependent in human liver.

(**A,B**) Kaplan-Meier survival curves of patients stratified by *SQSTM1* mRNA levels (z-score) in the TCGA (**A**) dataset and GSE10141 (**B**) are plotted with Log-Rank p value.

Supplemental Experimental Procedures

Mice experiments

DEN (25 mg/kg) was injected intraperitoneally (i.p.) into 14 days old male mice. After 4 weeks, mice were separated into two dietary groups and fed either LFD or HFD until sacrificed at 7-8 months of age. To generate STZ-HFD mice, 2 days-old male pups were injected with streptozotocin (200 μg) and placed on HFD from 4 week-old until sacrificed. These mice progress from NAFLD to NASH and develop HCC at 4-5 months of age. Mice were sacrificed and livers removed and separated into individual lobes. Externally visible tumors (>1 mm) were counted and measured. Large lobes were fixed in 10% formalin for 24-48 hr for paraffin blocks, or embedded in Tissue-Tek OCT compound (Sakura Finetek) for frozen block preparation. Frozen tissue sections were stained with Oil-Red O (ORO) for lipid, dihydroethidine (DHE) for ROS, and anti-smooth muscle actin (SMA) antibody (Abcam) or Sirius red for fibrosis detection. Paraffin-embedded tissues were used for H&E and IHC, except for SMA, staining. A board certified pathologist (M.A.V.) evaluated histological results. Positively stained areas were quantified in 6-10 random fields (×100, × 200 or x400) on each slide using Image J software and values are depicted in bar graphs next to the images. Scale bars: 100 μm. Remaining lobes were micro-dissected into tumor and non-tumor tissues and stored at −80°C until analyzed.

IB, IHC and other procedures

Liver samples were homogenized in RIPA buffer and equal amounts of homogenates were SDS-PAGE fractioned and transferred onto a PVDF membrane that was incubated, after blocking, with antibodies to phospho-AKT, phospho-ERK, ERK, LC3, NRF2 (all from Cell Signaling Technology), phospho-p70S6K, p70S6K, actin, HDAC1, TSC1 (all from Santa Cruz), Flag, tubulin (sigma), c-Myc (GeneTex), Nqo1 (Abcam) and p62 (Progen or Santa Cruz). IHC was performed as described (Nakagawa et al., 2014; Umemura et al., 2014). ALT and liver triglycerides were measured as described (Nakagawa et al., 2014).

Antibodies used for IHC in this study were against: phospho-S6, RelA, YAP, (Cell Signaling Technology), F4/80 (Caltag), c-Myc (GeneTex), Flag (sigma), AFP (Biocare medical), Sox9 (Santa Cruz), Glypican3, Nqo1 (abcam) and p62 (Progen). Sirius red staining was performed to quantify the amount of collagen fibers. ORO, Sirius red, SMA, F4/80, and DHE positive areas were quantified in 6-10 random fields (×100, × 200 or x400) on each slide using Image J software and the values are depicted in the bar graphs next to the images. Scale bars: 100 μm.

TCGA data

Raw data were downloaded from UCSC Cancer Genome Browser (Illumina Hiseq pancan normalized). GSEA of the correlation profile for *SQSTM1* was performed using pearson correlation with 1000 permutations against the C3 geneset compilation. Survival analysis was performed by patient stratification of *SQSTM1* z-score values.

Generation and infection of p62-AAV vectors

PCR amplified p62 sequences were cloned into pcDNA-Flag vector to add Flag-tag at the N-terminal end. The Flag-p62 constructs were subcloned into pEMBL-CB. Recombinant Flag-p62 was identified by enzyme digestion and sequencing, transfected into 293 cells, and its expression was IB analyzed. The ds-AAV8 vector was kindly provided by Dr. X. Xiao (University of North Carolina at Chapel Hill). Mice (6-8 weeks) were infected with p62 or GFP AAV vectors (2.8×10^{11} genome copies per mouse) via tail vein injection.

Statistical Analysis

Data are presented as means ± SD or ± SEM as indicated. Differences in means were analyzed by Student's t test and one-way ANOVA. Kaplan-Meier survival curves were analyzed by log rank test. p values < 0.05 were considered significant (*: $p < 0.05$, **: $p < 0.01$, ***: $p < 0.001$).

RNA Isolation and Real Time qPCR

RNA isolation from liver (20 mg) was performed using the RNeasy mini kit (Qiagen, Valencia, CA). Real time qPCR was used for quantifying mRNA concentrations using the SsoAdvanced™ Universal SYBR® Green Supermix (Irvine, CA) according to manufacturer's protocol. The primers used are as follows:

Nqo1	F	AGCGTTCGGTATTACGATCC
	R	AGTACAATCAGGGCTCTTCTCG
Hmox1	F	GAGCCTGAATCGAGCAGAAC

	R	AGCCTTCTCTGGACACCTGA
Col4a1	F	CTGGCACAAAAGGGACGAG
	R	ACGTGGCCGAGAATTTCACC
Col1a1	F	GCTCCTCTTAGGGGCCACT
	R	CCACGTCTCACCATTGGGG
Timp1	F	GCAACTCGGACCTGGTCATAA
	R	CGGCCCGTGATGAGAAACT
Acta2	F	GTCCCAGACATCAGGGAGTAA
	R	TCGGATACTTCAGCGTCAGGA
Areg	F	TCATGGCGAATGCAGATACA
	R	GCTACTACTGCAATCTTGGA
Ctgf	F	TGACCTGGAGGAAAACATTAAGA
	R	AGCCCTGTATGTCTTCACACTG
Afp	F	CAGCAGCCTGAGAGTCCATA
	R	GGCGATGGGTGTTTAGAAAG
Glypican3	F	TGTGGTCATGCAAGGCTGTA
	R	GGCACAGACATGGTTCTCAGG
Sqstm1	F	ATGTGGAACATGGAGGGAAGA
	R	GGAGTTCACCTGTAGATGGGT
Cd44	F	CAGAGGCGACTAGATCCCTC
	R	GAGTCACAGTGCGGGAACTC
Epcam	F	CGGCTCAGAGAGACTGTGTC
	R	GATCCAGTAGGTCCTCACGC
Gapdh	F	TTGATGGCAACAATCTCCAC
	R	CGTCCCGTAGACAAAATGGT
Gstm1	F	ATAGGTGTTGCGATGTAGCG
	R	TTCCCAAACCTGAGGGACTT
Gstm2	F	TGTCCTTGATCAACACCGAA
	R	TTCTTCAGGCCCTCAAAGC
Gstm3	F	AACACAGGTCTTGGGAGGAA
	R	AAACCTGAGGGACTTCCTGG
Gstm4	F	GCTGCTCCAAGTATTCCACC
	R	GACATTTTGGAGAACCAGGC
Gstm6	F	TCAAGAACTCTGGCTTCCGT
	R	GAGGATCCGTGTGGACATTT
Gstp1	F	GGGCCTTCACGTAGTCATTC
	R	GGATATGGTGAATGATGGGG
Gstp2	F	CTCCCTCTGGTTTTTCCCA

	R	CCCAAGTTTGAGGATGGAGA
Gsta1	F	CATTGAAGTGGTGAAGCACG
	R	CTGGACTGTGAGCTGAGTGG
Gsta2	F	TTGAAGTAGTGAAGCACGGG
	R	ATTGGGAGCTGAGTGGAGAA
Gclm	F	TTGGGAACTCCATTCATTCA
	R	CGGGAACCTGCTCAACTG
Gclc	F	TTCATGATCGAAGGACACCA
	R	CTGCACATCTACCACGCAGT
SQSTM1	F	AGCGTCTGCGAGGGAAAG
	R	ACCCGAAGTGTCCGTGTTT
MYC	F	CCTCGGATTCTCTGCTCTC
	R	TGGTGGTGGGCGGTGTCT
NQO1	F	GGTGATATTTCAGTTCCCATTGC
	R	GCAGGATGCCACTCTGAATC